Preferential removal of pesticides from water by molecular imprinting on TiO_2 photocatalysts

Roberto Fiorenza,[*a] *Alessandro Di Mauro,*[a] *Maria Cantarella,*[a] *Carmelo Iaria,*[b] *Elena Maria Scalisi,*[c] *Maria Violetta Brundo,*[c] *Antonino Gulino,*[d] *Luca Spitaleri,*[d] *Giuseppe Nicotra,*[e] *Sandro Dattilo,*[f] *Sabrina Carola Carroccio,*[a, f] *Vittorio Privitera,*[a] *and Giuliana Impellizzeri*[a]

[a] *CNR-IMM, Via S. Sofia 64, 95123 Catania, (Italy).*

[b] *Department of Chemical, Biological, Pharmacological and Environmental Sciences, University of Messina, Messina, (Italy).*

[c] *Department of Biological, Geological and Environmental Science, University of Catania, Catania (Italy).*

[d] *Department of Chemistry, University of Catania, and I.N.S.T.M. UdR of Catania, Viale Andrea Doria 6, 95125 Catania, (Italy).*

[e] *CNR- IMM, Z.I. VIII Strada 5, 95121 Catania, (Italy).*

[f] *CNR-IPCB, Via Paolo Gaifami 18, 95126 Catania, Italy.*

*** Corresponding author**

E-mail address: rfiorenza@unict.it

Abstract

In order to achieve a selective removal of specific pesticides from water, we synthesized, through the sol-gel technique, molecularly imprinted TiO_2 photocatalysts with the only use of the standard reactants for the TiO_2 sol-gel synthesis together with the pesticide molecules, without any addition of further reactants, supports or matrices. It is a new, easy, smart and scalable method that avoid the multistep and solvent-consuming procedures, typical of the molecular imprinting. Two widely-used pesticides, i.e. the herbicide 2,4D, and the insecticide imidacloprid, were chosen as template for the molecular imprinting and as contaminants target for the photocatalytic tests. A remarkable enhancement of the photocatalytic activity was verified with the TiO_2 imprinted with the corresponding pesticide-target. The selectivity of the photodegradation process was verified thanks to the comparison with the degradation of pesticides not-used as template. Furthermore, the eventual toxic effects of the molecularly imprinted materials were evaluated by biological tests.

The combination of molecular imprinting with photocatalysis, here investigated for the first time with pesticides, it is a promising strategy to selectively catch (through the molecular imprinting process) and degrade specific organic contaminants from water (through the photocatalysis).

Keywords: Photocatalysis, Titanium dioxide, Water purification, Pesticides, Molecular Imprinting.

1. Introduction

The intensification of agricultural practises to fulfil the ever-increasing global demand of food has generated, as side effect, an enhanced contamination of air, water, soil and aquatic ecosystems [1,2]. In this contest, one of the major problems of the last years is the pollution of surface and ground waters by pesticides. The harmful effect of these chemical compounds arises from their toxicity and from the high mobility and persistence in the aqueous media [3,4]. Generally, in fact, only a low percentage of the applied pesticides is able to protect the agriculture products, while the major portion of pesticides is lost in the environment through volatilization, hydrolysis, degradation by photolysis or by microbial action [5]. The negative consequence is the high cost of agricultural production with a heavily-polluted environment.

Heterogeneous photocatalysis is recently emerged as a totally-green technology for environmental applications [6-10]. In particular, titanium dioxide (TiO_2)-based photocatalysis is considered today an efficient methodology in the area of wastewater treatment [11-17] and for hydrogen production by photocatalytic water splitting [18,19].

TiO_2 (commonly called *titania*) is an abundant, inexpensive, and nontoxic semiconductor material. The production of hydroxyl radicals, formed by the interaction of oxygen and water with the photoelectron-hole pairs (generated after the exposure of TiO_2 to UV irradiation), allows to degrade a wide variety of bio-recalcitrant compounds [20,21]. Despite the countless advantages of the photocatalysis, one drawback is the non-selectivity of the process. Usually indeed, the water effluent streams contain a mixture of high toxic organic and non-biodegradable pollutants and less toxic organic and biodegradable compounds. Normally, the high toxic compounds are present in low concentrations, whereas the less toxic and biodegradable compounds are the major

components [22,23]. When TiO_2 is used to purify this type of water, the low and/or non-toxic organic contaminants at high concentrations are firstly removed, while the highly toxic organic pollutants at low concentrations are difficult to degrade. Furthermore, the selectivity of the photocatalytic process could be important in some industrial applications dealing with aqueous mixture containing compounds that should be removed and other compounds that should be recovered [24]. Therefore, the achievement of a selective TiO_2-based photocatalysis process is a fundamental task to obtain an efficient water remediation treatment.

Different methodologies have been investigated to enhance the selectivity of TiO_2, such as the pH variation [25,26] to control the surface electric charge, the surface functionalization with specific molecules that can afford a selective and effective adsorption of specific organic pollutants [27,28], the doping process [29, 30], or the modification of the crystallinity of the photocatalysts [31]. An innovative and effective strategy to design TiO_2 photocatalyst able to enhance the selectivity degradation of the organic contaminants can be obtained by the molecular imprinting (MI) process.

Since the first work of M. V. Polyakov in 1931 [32], the molecular imprinting technique has been recognized as a performing method to produce materials with a memory of the size, shape, and chemical composition of the template molecules [33-37]. The synthesis method consists in favouring the interaction of the template molecules onto an organic or inorganic matrix during its preparation step; a subsequent removal of the imprinted molecule (i.e., the template) leads to cavities complementary to the template. The combined approach between molecular imprinting and photocatalysis leads to obtain a selective photodegradation; in detail, the molecular imprinting process promotes a selective interaction between the TiO_2 and the dangerous contaminant,

whereas the photocatalytic process, activated by the titanium dioxide, efficiently degrades the specific pollutant.

Until now, there are some studies in the literature that analyse the performance of TiO_2 nanoparticles coated or supported with a layer of molecularly imprinted polymers (MIP). These materials exhibited specific affinity toward various target pollutants [38-43]. However, this approach has still some drawbacks. First of all, the synthesis of these imprinted photocatalysts usually required multistep procedures, needed for the preparation of the polymer matrix, which involve a relevant consumption of time and solvents; additionally, the polymeric matrix can cover the surface active sites of TiO_2, hindering the light absorption and thus decreasing the photocatalytic activity; finally, the removal of the template from the polymer matrix can be sometimes difficult, due to the strong chemical interaction that can be formed between the polymer and the target molecules. To avoid such disadvantages, the development of materials with a molecularly imprinted inorganic framework (namely, without the utilize of organic polymers) can be a successfully strategy. Silica (SiO_2) has been used as the inorganic matrix [44-47]. An alternative methodology consists in synthesizing TiO_2 without the use of a supporting matrix, adding in the first step of the titania synthesis the target pollutant and then removing it with a thermal treatment. This process allows to obtain a molecularly imprinted TiO_2. This procedure is simple and environmental-friendly: the imprinted cavities can be shaped during the synthesis of titania, and the template molecules can be totally removed by calcination. To our knowledge, only few papers have reported this approach for the synthesis of imprinted TiO_2 photocatalysts as nanoparticles or as films [48-51], and no one has investigated the photocatalytic water purification from pesticides. Additionally, the selection of pesticides as target pollutants in the photocatalytic experiments are less investigated in the literature compared to other

molecules (such as, dyes or phenolic compounds), due the harder reaction conditions required for these type of contaminants [52, 53].

On the above considerations, we here report for the first time the experimental results of the preferential photodegradation of two widely used pesticides: the herbicide 2,4-dichlorophenoxyacetic acid (2,4D), and the insecticide imidacloprid (1-(6-chloro-3-pyridinylmethyl)-N-nitro-2-imidazolidinimine), using molecularly imprinted TiO_2 catalysts synthesized towards the sol-gel technique without the addition of organic or inorganic matrix.

The 2,4-D (Fig. 1, molecular length: 1.002 nm, estimated by ChemDraw©) belongs to the group of synthetic chlorophenoxy herbicides. It can be also used in combination with other herbicides for the post-emergence control of broad-leaved weeds [54]. It persists in the environment for a long time [55], and it has been identified by the International Agency for Research on Cancer as a possible human carcinogen (class 2B-carcinogen) [56]. The imidacloprid (Fig. 1, molecular length: 1.078 nm, estimated by ChemDraw©) is a neonicotinoid insecticide having outstanding effectiveness and systemic action for crop protection against piercing-sucking pests. The wide use of imidacloprid causes, for its high leaching potential [57], soil pollution, surface/underground water contamination, and destruction of biological systems [58]. Severe exposure to imidacloprid can cause thyroid lesions, lethargy and spasms, and it can harm the mammalian reproduction [59,60].

The photocatalysts were characterized by scanning electron microscopy (SEM), transmission electron microscopy (TEM), X-ray diffraction (XRD), N_2 adsorption-desorption measurements, Fourier Transform Infrared (FTIR), X-ray photoelectron (XPS), UV-vis diffuse reflectance spectroscopy (DRS), and point of zero charge (pzc) determination.

The toxicity of the samples was assessed by the zebrafish embriotoxicity test (ZFET), according to the Organization for Economic Co-operation and Development (OECD, 2013) [61]. ZFET is a modern non-animal test, representing an effective alternative to acute test with adult fish. [62] Moreover, it is an excellent test for the valuation of toxicity of micro/nanoparticles [63-65]. The metallothioneins 1 (MTs1), a group of low molecular mass proteins, were analysed as biomarkers of exposure. These proteins are involved in heavy metal ion homeostasis and detoxification [66].

2. Experimental

2.1. Catalyst preparation

Titanium(IV) butoxide, 2,4-dichlorophenoxyacetic acid (2,4D) and imidacloprid, were purchased from Sigma-Aldrich; ethanol and glacial acetic acid from VWR. All the chemical substances were used without any further purification. The molecularly imprinted TiO_2 samples were synthetized using the sol-gel technique [67]. The stoichiometric amount of pesticide required to obtain a molar ratio of 5:1 between TiO_2 and 2,4D or imidacloprid was dissolved in a solution of 0.5 ml of acetic acid and 1.5 ml of ethanol; then the solution was stirred at room temperature until a complete solubilization of the pesticide. Successively, 2 ml of titanium butoxide was added in the mixture and it was stirred for further 10 min. Then, a solution containing 2 ml of demineralized water, 2 ml of acetic acid and 2 ml of ethanol was added dropwise to the above solution. The resultant slurry was stirred for 3 hrs and aged for 24 hrs. The obtained wet gel was dried at 100 °C for 12 hrs and then calcined in air at 500 °C for 6 hrs (heating ramp 2 °C/min) to remove the template/pesticide molecules and the organic substances formed during the synthesis. The samples will be hereafter called "TiO_2 MI/2,4 D" and "TiO_2 MI/Imid". The imprinted titania without the calcinations process

will be identified as "TiO_2 MI/2,4 D Not Removed" and "TiO_2 MI/Imid. Not Removed". The bare TiO_2 (simply called "TiO_2") was prepared with the same procedure described above without the use of pesticides.

2.2. Catalyst characterization

The morphology of the synthesized samples was investigated by SEM with a field emission Zeiss Supra 25 microscope, and by TEM with a JEOL ARM200F Cs-corrected, operated at 200 keV. In more detail, the TEM images were acquired in Bright Field TEM mode (BF-TEM) and high resolution mode (HR-TEM). The X-ray diffraction (XRD) analyses were performed with a Bruker D-500 diffractometer, operating with a parallel Cu-Kα radiation at 40 kV and 40 mA, 2θ from 20° to 60°, in grazing incidence mode (0.8°). The XRD patterns are reported in counts per second (cps) versus 2θ, and they were examined by the Bruker software suite, including ICSD structure database. The textural properties of the materials were determined by Brunauer-Emmett-Teller (BET) adsorption-desorption of N_2 at -196 °C using a Micromeritics Tristar II Plus 3020 with a pre-treatment of out-gassing at 100 °C overnight. The FTIR spectra were obtained through a Perkin-Elmer Spectrum 1000 spectrometer (accuracy of wavenumber ± 0.01 cm^{-1}, resolution 4 cm^{-1}). The investigated samples, in the form of tables, were obtained by mixing the catalysts powders (1 mg) with KBr powders (300 mg) in an Agate mortar and pressing with a press. The XPS analyses were performed at 45° take-off angle relative to the surface plane with a PHI 5600 Multi Technique System (base pressure of the main chamber: 1×10^{-8} Pa) [68, 69]. Samples were excited with Al Kα X-ray radiation using a pass energy of 5.85 eV. Structures due to the Kα satellite radiations were subtracted from the spectra prior to data processing. The XPS peak intensities were obtained after Shirley background removal [68,69]. The atomic concentration analysis was performed by taking into

account the relevant atomic sensitivity factors. The instrumental energy resolution was ≤ 0.5 eV. Spectra calibration was achieved by fixing the main C 1s signal at 285.0 eV. The point of zero charge (pzc) of the catalysts was established with the Noh-Schwarz method of mass titration [70]. This method involves to find the asymptotic value of the pH of an oxide/water slurry as the oxide mass content is increased. The typical values of oxide/water by weight were 0.1, 1, 5, 10, 20, 40%. DRS spectra were recorded in the 200-700 nm wavelength range, using a Perkin-Elmer Lambda 40 UV-vis spectrophotometer.

2.3. Photocatalytic activity experiments

The selective photodegradation of 2,4D and imidacloprid pesticides were investigated under UV irradiation using an UV lamp centred at 368 nm (emission spectrum showed in the Fig. S1C), with a full width at half maximum lower than 10 nm, and an irradiance of 4 mW/cm^2, which simulate the UV irradiance of the sun on the Earth. Prior to carry out the measurements, the catalysts were irradiated by the UV lamp for 60 min in order to remove the hydrocarbons and the adventitious carbon from the samples' surface [71]. A quantity of 1 mg of catalyst powders was immersed in 4 ml of aqueous solution of 2,4D or imidacloprid in quartz cuvettes. The starting concentration of 2,4D and imidacloprid was fixed to 5×10^{-5} M for both organic contaminants. The solutions were treated by ultrasonic irradiations with a frequency of 50 Hz for 5 min, to favour the dispersion of the powders. Control experiments were carried out in the dark for 90 min to ensure the adsorption-desorption equilibrium of the pesticides on the beaker's surface and on the samples' surface. At regular time intervals (for a total time of 3 hrs), 2 ml of the irradiated solutions were measured with an UV-vis spectrophotometer (Lambda 45, Perkin-Elmer), in a wavelength range of 200-700 nm. Before any measurements, the samples were centrifuged for 3 min with a spin of 1500

rpm, to remove the powders and reduce the light scattering phenomena during the spectrophotometric measurements. The degradation process of 2,4D and imidacloprid was evaluated by the absorbance peaks at 229 nm and 270 nm (Figs. S1A-B), respectively, in the Lambert-Beer regime [72]. The degradations of 2,4D and imidacloprid in the absence of any photocatalyst were also valuated as references.

The photocatalytic tests in presence of a mixture solution of 2,4D and imidacloprid (2 ml 2,4D 5×10^{-5} M + 2 ml imidacloprid 5×10^{-5} M) were also investigated, following the same experimental conditions reported above.

The selectivity of the photodegradation process was verified thanks to the comparison with the degradation of the pesticides not-used as template, and also using another pesticide: the fungicide ortho-phenylphenol (5×10^{-5} M).

The mineralization of the 2,4D and imidacloprid pesticides after the photocatalytic process was evaluated by measuring the total organic carbon (TOC) content with a Shimadzu TOC-LCSH analyzer (tested volume: 3 ml) equipped with a non-dispersive infrared detector. The inorganic carbon was removed from the tested solutions using the Non-Purgeable Organic Carbon (NPOC) method by adding phosphoric acid and successively purging by dry air, then the TOC content was measured after a high-temperature catalytic oxidation at 680 °C.

The photodegradation products were determined by the Electrospray Ionization (ESI) mass analysis. The measurements were performed by a Thermo Finnigan LCQ-DECA ion trap mass spectrometer (Thermo Fischer Scientific, San Jose, CA), equipped with an Atmospheric Pressure Ionization (API) source. Mass spectra were acquired in negative ion mode in the m/z range 150-225 under the following conditions: capillary temperature 130 °C nebulizer gas (nitrogen) with a flow rate of 15 arbitrary units; source voltage 4 kV; capillary voltage 46 V; tube lens voltage 90 V. After

photocatalysis, each solution was injected (direct infusion) into the mass spectrometer, at a flow rate of 10 μL/min. The mass spectrometer was calibrated using a standard mixture sodium dodecyl sulfate (265.17 Da), Ultramark (1621 Da) and sodium taurocholate (514,42 Da).

2.4. Zebrafish embriotoxicity test

In order to test the eventual toxicity of the synthesized materials, zebrafish eggs fertilized within 4 hrs post fertilization (hpf) were provided from the Center of Experimental Ichthyiopathology of Sicily (CISS), University of Messina (Italy). Zebrafish embryos were exposed to bare TiO_2, and to test the eventual toxicity changes due to the molecular imprinting process, to the TiO_2 MI/Imid, used as model sample for the molecularly imprinted TiO_2 materials. Two concentrations (14×10^{-5} and 14×10^{-6} mg/ml) in 5 ml of freshwater for 4-96 hpf were measured for evaluating the possible toxic effects of the synthesized powders on the zebrafishs. The solutions were renewed and embryonic/larval mortality and hatching rate were evaluated every 24 hrs. According to *Ref.* [65], healthy embryos were placed in 24-well culture plates (10 embryos in 5 ml solution/well). Each group had five replicate wells. Each experiment was repeated four times. Two larvae of each group were used for immunodetection of biomarkers by immunofluorescence according to *Ref.* [73]. The primary antibody anti-mouse-methallotionein 1 (1:500, from Abcam) and secondary antibody with fluorescein tetramethylrhodamine (TRITC) conjugated goat anti-mouse IgG (1:1,000, form Sigma-Aldrich) were used. Negative controls were performed by incubation with anti-mouse sera without antibodies. Observations were carried out using confocal laser scanning microcopy (CLSM; Zeiss LSM 700), equipped with the ZEN-2011 software and with a red fluorescence filter set.

3. Results and discussion

The SEM images of TiO_2, TiO_2 MI/2,4D and TiO_2 MI/Imid powders are reported in Fig. 2. All the samples showed a rough morphology with heterogeneous shaped particles. The non-homogenous morphology is typical of the TiO_2 matrix-free sol-gel synthesis [74-76]. The inset of Fig. 2A depicts a high magnification of the material.

The TEM analyses (Fig. 3 and S2) performed on TiO_2 and TiO_2 MI/2,4D samples evidenced a granular morphology, irrespective of the molecular imprinting process. The diffraction pattern of the TiO_2 sample (inset of Fig. 3A) unequivocally showed a polycrystalline anatase phase of the synthesized titania, in good agreement with the literature [77]. The diffraction pattern obtained for the TiO_2 MI/2,4D (inset of Fig. 3B) does not show any change in the crystalline structure, due to the molecular imprinting process.

XRD analyses are reported in Fig. 4. All the XRD patterns are typical of the TiO_2 in the anatase phase (JCPDS number 21-1272), as confirmed by the signal at 2θ = 25.3° (101), 37.8° (004), 38.5° (112), 48.0° (200), 54.0° (105), and 55.1° (211), and in agreement with the TEM analyses (insets of Fig. 3), consequently the diffraction analyses do not evidence substantial modifies in the crystalline structure of molecularly imprinted samples with respect to the reference one (i.e., TiO_2).

Some interesting variations in the textural properties were highlighted through the N_2 adsorption-desorption measurements. All of the samples exhibited the type-IV isotherm (not shown) typical of a mesoporous structure, as expected [78]. Table 1 reported the BET surface area (S_{BET}), the mean pore diameter (d_p), and the pore volume (V_p) of the investigated samples. The BET surface area of the bare TiO_2 is 59 m^2/g and the molecular imprinting process caused a decrease of surface area of 4 m^2/g for the TiO_2

MI/2,4D and of 6 m^2/g for the TiO_2 MI/Imid. Consequently, an increase in the mean pore diameter and in the pore volume was detected compared to un-modified TiO_2 (Table 1). The BJH (Barrett, Joyner and Halenda) method [79] was used to calculate the pore size distributions of the samples from experimental isotherms. Fig. 5 reports the differential variation of the pore volume per pore unit as a function of the pore diameter. A clear shift towards larger pores is detected due to the molecular imprinting process. In detail, the TiO_2 MI/Imid catalysts exhibited the largest distribution, with a mean pore diameter of 9.7 nm (Tab. 1), about 4 nm larger than the mean pore diameter of the TiO_2 MI/2,4D catalyst, and about 5 nm larger than the mean pore diameter of bare TiO_2. The differences in the textural properties between the bare TiO_2 and the molecularly imprinted samples can be reasonably due to the molecular imprinting process which induces the modifications of the pores already existing in the structure of the not-imprinted TiO_2.

FTIR measurements were carried out to check the effectiveness of the molecular imprinting process. The FTIR results are reported in Fig. 6. In particular, Figure 6A displays the FTIR spectra of 2,4D, TiO_2 MI/2,4D Not Removed (i.e. before the calcination), TiO_2 MI/2,4D, and TiO_2. The 2,4D pesticide showed a peak at 1736 cm^{-1} which is related to the presence of C=O of the carboxyl group [80]. The peaks at 1478 cm^{-1} and 1431 cm^{-1} indicates the C=C vibrations of the aromatic ring and the CH_2 vibrations of alkanes, respectively [80,81]. The antisymmetric and symmetric vibrations of C−O−C correspond to the bands at 1312 cm^{-1} and 1092 cm^{-1}, whereas the band at 1230 cm^{-1} is due to O−H vibration coupled with C−O stretching [82]. The peak at 642 cm^{-1} is attributed to C−Cl stretching [83]. The TiO_2 MI/2,4D Not Removed exhibited some of the typical bands of 2,4D which indicate the successful attachment of the molecule target (2,4D) to the titanium dioxide. Specifically, as reported in Table 2, the

bands at 1736 cm^{-1}, 1312 cm^{-1}, and 1092 cm^{-1} of 2,4D are shifted to different wavenumbers on the TiO_2 MI/2,4D Not Removed. These shifts can be correlated to the formation of hydrogen bonding and to the electrostatic interactions originated during the first steps of the sol-gel synthesis, i.e. the hydrolysis and the successively condensation of titanium butoxide [49]. Indeed, the first step of sol-gel synthesis involved the hydrolysis of titanium butoxide with the consequent condensation to form the Ti-O-Ti network. Meanwhile, the formation of the complex between TiO_2 and the pesticide (added together to titanium butoxide) occurs by electrostatic interaction and hydrogen bonding. The calcination treatment leads to the complete removal of the pesticide and the consequently formation of the molecularly imprinted sample, as confirmed by FTIR spectrum of the TiO_2 MI/2,4D sample, in which the bands related to the 2,4D are absent. Indeed, the spectrum of the TiO_2 MI/2,4D catalyst is almost similar to that of bare TiO_2. The wide band in the range 700-500 cm^{-1} observed for the TiO_2 MI/2,4D and TiO_2 samples can be assigned to the Ti−O−Ti stretching vibration modes [82]. The band at 1628 cm^{-1} of un-modified TiO_2 is assigned to the bending vibration of the O−H group of residual water molecules.

The FTIR spectra of imidacloprid, TiO_2 MI/Imid Not Removed (i.e., before the calcination), TiO_2 MI/Imid, and TiO_2 are shown in Fig. 6B. The bands at 3363 cm^{-1} and 1288 cm^{-1} of imidacloprid are assigned to the stretching of N−H and N−C of secondary ammine, respectively [83]. The peak at 1569 cm^{-1} characterizes the stretching vibration of pyridine ring, whereas the band at 1445 cm^{-1} are attributed to the C=N ring in-plane vibrations and to the deformation modes of =CH− on the pyridine ring [84]. The symmetric vibration of NO_2 group can be identified with the band at 1230 cm^{-1}, whereas the asymmetric vibrations that are usually associated to the bands in the 1530-1630 cm^{-1} region overlap with the other bands related to the stretching vibration of pyridine ring

(reported in the 1500-1300 cm^{-1} region) [85]. Finally, the band at 1051 cm^{-1} is assigned to pyridine C−Cl stretching [82]. Also in this case the TiO_2 Imid Not Removed sample (i.e., without calcination treatment) showed some fingerprint bands of the pesticide used as template, whereas as expected after the calcination (TiO_2 MI/Imid sample) the peaks due to the presence of imidacloprid disappeared. Table 3 indicates a shift from 1569 cm^{-1} for imidacloprid to 1539 cm^{-1} for TiO_2 MI/Imid Not Removed, due to the electrostatic interactions and the hydrogen bonds with the nitrogen of pyridine of imidacloprid, confirming also for these samples the successful attachment of the target molecule (i.e., imidacloprid) to the Ti−O−Ti network in the first steps of sol-gel route. The wide band at 3358 cm^{-1} of TiO_2 MI/Imid Not Removed could be due to the overlap of the peaks of the stretching of amine group and the peaks of the stretching of the adsorbed water. The TiO_2 MI/Imid sample displayed the typical FTIR spectrum of titanium dioxide, unambiguously demonstrating the removal of the template thanks to the calcination process.

In order to have further validations of the successful interaction between the pesticides and the TiO_2 and to exclude the eventual presence of other elements/impurities on the samples' surface, XPS measurements were carried out (Fig.7). Stoichiometric TiO_2 samples are white in colour, while the eventual presence of oxygen deficient TiO_{2-x} species causes changes in colouration from white up to deep blue in TiO_2 ceramic samples [86,87]. All the samples prepared in this study were white. As an initial check control, we performed XPS analysis of bare TiO_2 anatase powders. XPS results show the Ti $2p_{3/2,\ 1/2}$ spin-orbit components at 459.9 and 465.6 eV (Tab. 4, Fig. S3A) and a rather symmetric O 1s band at 531.1 eV (Fig. S3B), in agreement with already reported literature data for the anatase phase [88]. No evidence of low binding energy broadening of the doublet evident for TiO_2 itself was observed. This fact

suggests the substantial absence of TiO_{2-x} species on the XPS probed depth [86, 87]. In fact, the eventual presence of Ti ions in a 3+ valence state should give origin to an XPS spectrum consisting of a pair of overlapping Ti 2p doublets, because of the competition of various final state screening effects [89-91].

The XPS spectrum of the TiO_2 MI/2,4D Not Removed sample (i.e., before the calcination) shows the Ti 2p 3/2 and ½ spin-orbit components at 459.3 and 465.2 eV (Tab. 4, Fig. S3C), and a rather broad O 1s band centred at 531.7 eV (Tab. 4, Fig. S3D). The Ti 2p levels are at 0.6-0.4 eV lower binding energies with respect to those observed for the not-imprinted TiO_2, thus indicating the donation electron capability of the 2,4D molecule. In contrast, the O 1s spectral profile clearly suggests the presence of different electronic states consistent with the presence of TiO_2, oxygen atoms belonging to the 2,4D molecule, water and, finally, Ti-OH hydroxide species.

Fig. 7A shows the XPS spectrum of the TiO_2 MI/2,4D sample (i.e after calcination at 500 °C) in the Ti 2p energy region. The Ti 2p features are at 459.4 eV and 465.2 eV (Tab. 4). These XPS values are almost coincident with those observed for the TiO_2 MI/2,4D Not Removed sample, thus suggesting that the calcination process does not significantly modify the electronic states of the imprinted system. It seems that after calcination a “memory” effect maintains the overall electronic structure, thus confirming the retention of the structural microstructure of the pesticides molecules. Worthy of note, while the TiO_2 MI/2,4D Not Removed sample clearly shows (Fig. S4A) the Cl 2p spin-orbit components at 200.2 and 201.7 eV (Tab. 4), (in close agreement with the XPS values observed for the 2,4D molecule), in contrast there is no XPS trace of chlorine (Cl 2p states) after the calcination. These observations demonstrate the absence of the 2,4D molecule (Fig. S4A) in the TiO_2 MI/2,4D sample. Moreover, Fig. 7B illustrates the highly symmetric O 1s XPS band of the TiO_2 MI/2,4D catalyst. It is evident that the

calcination procedure removes also both water and Ti-OH hydroxide surface contaminants.

XPS ionization energies, related to the TiO_2 MI/Imid Not Removed (Figs. S4 B-C) and TiO_2 MI/Imid (Figs. 7C-D) samples, are strongly reminiscent of those of the TiO_2 MI/2,4D system, being the former ionization just about 0.3 eV at lower binding energies (Tab. 4). This evidence demonstrates the electron donating capability of this further molecule (imidacloprid) and the fact that the calcination procedure does not significantly modify the electronic states of the imprinted samples (see Tab. 4). Furthemore, in the TiO_2 MI/Imid Not Removed sample the XPS N 1s band (Fig. S4D) clearly consists of two major evident features at 399.6 eV with a shoulder (due to the amine and imine moieties) at 405.3 eV (due to the $–NO_2$ group). In tune with the behaviour already observed for the TiO_2 MI/2,4 D catalyst, also in this case the calcination treatment totally removes the imidacloprid molecule from the TiO_2 matrix, since no XPS N 1s signal can be found in the related spectrum (Fig. S4D).

The results of the atomic concentration calculated by XPS analysis indicate that for all the calcined samples the O/Ti ratios are 2.2 ± 0.1, in agreement with the expected stoichiometry ratio. In contrast, the two not-treated samples (before calcination) show O/Ti ratios of 2.5 (TiO_2 MI/2,4D Not Removed) and 2.6 (TiO_2 MI/Imid Not Removed). These ratios are in agreement with the presence of oxygen atoms in both the 2,4D and imidacloprid pesticides. The nitrogen atomic concentration observed in the TiO_2 MI/Imid Not Removed catalyst gave a N/Ti ratio of 0.56, thus about a half with respect to the nominal concentration of nitrogen considering the 5 nitrogen of imidacloprid and the 5:1 molar ratio between the TiO_2 and the pesticides. Similar observations can be done for the TiO_2 MI/2,4D Not Removed sample that shows a Cl/Ti ratio of 0.32 close to the nominal ratio once the fact that the 2,4D molecule contains 2 chlorine atoms. On

the contrary carbon is present in all samples. This is expected, since it is well known that atomically pure TiO_2 samples can only been obtained by firing overnight at 1000 °C directly in the XPS main chamber, to avoid any contact with air before the XPS analysis [86,87]. We cannot perform this procedure since firing of TiO_2 at temperatures equal or above 600 °C causes the transformation of the anatase in the rutile phase. Moreover, the adventitious carbon contamination, due to the hydrocarbons present in air, is currently used to calibrate the XPS spectra [68, 69]. As a consequence, all the calcined samples contain a certain amount of carbon in the 5-10 % range. However, in accordance with the procedure reported in the literature [71] the catalysts were irradiated with UV radiation before the photocatalytic tests for 60 min, to remove the hydrocarbons and the adventitious carbon from their surface.

The absence of other impurities after the calcination process on the imprinted samples were further assed by the point of zero charge determination and the UV-vis DRS measurements. In particular, as showed in the Fig. S5 our materials did not exhibit any substantial variation of the point of zero charge due to the imprinting process, being the pzc between 6.7 ± 0.3 and 6.9 ± 0.3, also comparable to the values reported in the literature for the TiO_2 synthetized by sol-gel method [92, 93]. Similarly, only slight variations of the reflectance were detected in the imprinting samples compared to un-modified TiO_2 (Fig. S6), and the differences of band-gap values (from 3.0 ± 0.3 to 3.1± 0.3 eV) estimated by the Kubelka-Munk method [94] are included in the experimental error, suggesting that the molecular imprinting process did not modify the band-gap structure of TiO_2.

To test the photocatalytic efficiency of the synthetized samples, the degradation of 2,4D (Fig. 8A) and of imidacloprid (Fig.8B) pesticides under UV light irradiation was measured. The graphs report C/C_0 ratio as a function of time t, where C is the

concentration of the pollutant after UV light irradiation at the time *t*, while C_0 is the starting concentration of the pesticide (the variations of absorbance with the time are displayed in Fig. S7). The experimental error of the photodegradation measurements is 1%. Before the catalytic measurements, control experiments without irradiation, were performed. The results obtained in the dark did not indicate any relevant contribution of the adsorption process; this is probably related to the formation of weak interactions between the pesticides and the molecularly imprinted samples in the aqueous solution. Similar results, concerning the lack of contribution of the adsorption process, are reported in the literature for molecularly imprinted ZnO and TiO_2 [36, 48].

Fig. 8A is focused on the degradation of the 2,4D herbicide. In absence of any catalysts there is not a detectable degradation of 2,4D, as expected. Differently, bare TiO_2 sample leads to a degradation of the 2,4D pesticide of ~ 15%. A significant enhancement of the 2,4D conversion, till to ~ 47%, was obtained through the TiO_2 MI/2,4D catalyst. Thus, the combination of molecular imprinting with the photocatalytic process allowed to efficiently promote the 2,4D degradation compared to bare TiO_2 by a factor of ~ 3. A similar catalytic behaviour can be noted between the TiO_2 MI/Imid, and the un-modified TiO_2, that is an indication of an achieved selectivity in the photocatalytic process. Indeed, only the sample imprinted with the same pollutant that should be degraded (in this case the 2,4D pesticide that was imprinted on the TiO_2 MI/2,4D catalyst) can efficiently remove the 2,4D herbicide from the contaminated water. The calculated kinetic rate constants for all the investigated samples (considering a first order kinetic) [95,96] are reported in Tab. 5. The kinetic constant of TiO_2 MI/2,4D is ~ 6 times higher compared to the not-imprinted TiO_2 samples; this higher degradation rate of TiO_2 MI/2,4D is an evidence of the synergism between the molecular imprinting and the photocatalytic process: the former leads to selectively

catch (through the molecular imprinting process) the pesticide, the latter to effectively degrade it from water (through the photocatalysis).

It is important to remark that the high performance of the TiO_2 MI/2,4D catalyst cannot be related to any variation of the BET surface area. Indeed, the data reported in Tab. 1 indicate a similar surface area between bare TiO_2 (59±1 m^2 g^{-1}) and molecularly imprinted materials: TiO_2 MI/2,4D (55 ± 1 m^2/g) and TiO_2 MI/Imid (53 ± 1 m^2/g). Consequently, the key factor in the preferential photodegradation of the target pollutant is due to the molecular imprinting process.

The high performance through the photocatalytic oxidation of 2,4D pesticide showed by the TiO_2 MI/2,4D catalyst is promising to effectively remove this harmful compound from water. Underlining that the photo-oxidation can be considered and alternative solution together with adsorption [97, 98], the selective separation and sensing [99-101] obtained with other molecularly imprinted 2,4D materials.

The selectivity of the process was further confirmed considering the photoactivity of TiO_2 MI/2,4D towards the degradation of another pesticide: the imidacloprid insecticide. The result is reported in Fig. 8B. A comparable photoactivity was measured between the TiO_2 MI/2,4D and the un-modified TiO_2, highlighting the selectivity of the process. The TiO_2 MI/2,4D sample, in fact, due to the different pores/cavities and the dissimilar chemical composition of the 2,4D respect to imidacloprid, it is not selective for the imidacloprid degradation, showing the same catalytic activity of not-imprinted TiO_2.

Fig. 8B reports the degradation of the imidacloprid insecticide. Also for the photodegradation of the imidacloprid the molecular imprinting process allows to achieve a selective removal of this pesticide from water (the variations of absorbance with the time are showed in Fig. S8). The concentration of imidacloprid remains substantially the

same in the test without catalyst, while the TiO_2 degrades ~ 19% of the initial concentration of the imidacloprid pesticide. The TiO_2 MI/Imid showed the best activity, with a degradation of ~ 35%. Tab. 6 indicates a 2 times higher kinetic constant for TiO_2 MI/Imid compared to bare TiO_2. Only the TiO_2 MI/Imid catalyst (sample imprinted with the same pesticide/target to be degraded) allows to significantly increase the photocatalytic degradation of imidacloprid, confirming the attained selectivity of the process and the synergism between the molecular imprinting and the photocatalysis. Also in this case, the high performance of the TiO_2 MI/Imid catalyst cannot be related to any variation of the BET surface area (see Tab. 1). The modification, with the molecular imprinting process of the pores/cavities of TiO_2, is the key factor to obtain selective and performing materials. The modified pores/cavities are, indeed, the recognition sites for the selective interaction between the TiO_2 and the pesticides that favour an increased photoactivity.

In order to evaluate the ability in removing organic pollutants from the solution, we have measured the TOC amount of the pesticides solutions after 3 hours under UV irradiation. Figs. 8C and D suggested a partial mineralization of the solutions. These data are in good agreement with the photocatalytic mechanisms reported in the literature for the degradation of 2,4D and imidacloprid [95,96,102-104]. In particular, for the 2,4D pesticide, the hydroxyl radicals ($^{\bullet}OH$) (formed after the UV irradiation of TiO_2) react with the herbicide to yield mainly 2,4-Dichlorophenol and 2-chloro benzoquinone. This was confirmed by ESI-MS measurement reported in Fig. S9.

Regarding the TiO_2-driven imidacloprid photodegradation, it is expected that the interaction of the hydroxyl radicals with the imidacloprid gives the cleavage of C–N and the N–N bonds with the formation of amine and chloro-pyridine species [96,104].

Further oxidation processes lead to the formation of small molecules as H_2O, CO_2, chlorine dioxide and nitrogen oxides species [96,104].

The synthetized TiO_2-based photocatalysts exhibited a good reusability property (Fig. 9). Indeed, both the 2,4D photodegradation kinetic constant (Fig.9A) and the imidacloprid photodegradation kinetic constant (Fig.9B) remain essentially the same after five consecutive photocatalytic tests. The slight decrease of the kinetic constants in the last runs can be reasonably ascribed to a small loss of the powder during the centrifugation processes. Furthermore, no substantial variations were detected from the XPS and the FTIR analyses of the used (i.e after the photocatalytic tests) TiO_2 MI/2,4D and TiO_2 MI/Imid. (Figs. S10-S11) materials, confirming the stability of the investigated samples.

An additional photocatalytic test was performed, employing a mixed aqueous solution of 2,4D and imidacloprid. The results of this test are shown in Fig. 10 (the absorption spectra of the catalysts as a function of the time are reported in Fig. S12) Fig. 10A demonstrates that also in this case only the TiO_2 MI/2,4D leads to a higher performance in the photo-oxidation of the herbicide 2,4D. In detail, the kinetic constant of the 2,4D degradation is about 5 times higher compared to TiO_2 and TiO_2 MI/Imid (Tab. 7). Analogously, following the imidacloprid degradation in the mixed solution (Fig. 10B) it is clear that the TiO_2 MI/2,4D and TiO_2 exhibited similar photoactivity, whereas the TiO_2 MI/Imid effectively degrades the corresponding pesticide/template with a kinetic constant which is about 2 times higher compared to the ones of the other TiO_2 photocatalysts.

We performed a photocatalytic test with another pesticide: the fungicide ortho-phenylphenol. The molecular structure of the fungicide is reported in Fig. 11A. Fig. 11B shows that the imprinted samples displayed a similar catalytic behaviour of bare TiO_2

with comparable kinetic constants (Tab. 8). Indeed, being the molecular structure of the fungicide (Fig. 11A) completely different from the ones of 2,4D and imidacloprid (Fig. 1), no particular interactions between the imprinted samples and the pesticide are favoured, leading to a degradation rate similar to bare TiO_2.

Finally, to have further proofs of the selectivity of the synthetized TiO_2 molecularly imprinted samples, we carried out a photocatalytic test using the 1,4-dichlorobenzene pollutant, that has a similar chemical structure of 2,4D pesticide (Fig. 12A). It is possible to notice (Fig. 12B) that, also in this case, all the investigated catalysts showed similar performance, with a slightly better degradation efficiency displayed by the TiO_2 MI/2,4D (42%) compared to TiO_2 (37%) and TiO_2 MI/Imid (35%). The small increase of the photoactivity of the TiO_2 MI/2,4D can be due to the weak interactions occurring between this photocatalyst and the 1,4-dichlorobenzene caused by the chemical similarity between 1,4-dichloreobenzene and 2,4D. While the TiO_2 MI/Imid, owing completely different recognition sites/pores, exhibited the same catalytic behaviour of the un-imprinted TiO_2. As clearly visible from the Fig. 12B a small photodegradation due to the photolysis (i.e. degradation without catalysts), under UV irradiation, characterized the 1,4-dichlorobenzene, this is in accordance with the literature [105].

The reported photocatalytic tests indicate that the molecular imprinting process is as an effective methodology to achieve a selective degradation of pesticides from water by titanium dioxide. The samples synthesized using as templates the pesticides showed a remarkable catalytic activity towards the corresponding pesticide (i.e. TiO_2 MI/2,4D towards 2,4D; TiO_2 MI/Imid towards imidacloprid). This is due to the electrostatic interactions and hydrogen bonds formed during the sol-gel synthesis between the Ti−O−Ti network and the pesticide molecules (as confirmed by FTIR analyses reported in Fig. 6). After calcination, the pesticide is completely removed (as confirmed by FTIR

analyses depicted in Fig. 6, and confirmed by XPS results reported in Fig. 7) from the TiO_2, favouring in this way the formation of a titania with a "memory" of the template molecules. The final result is a specific molecular recognition between the molecularly imprinted TiO_2 and the pesticide used during the synthesis step. This allows a selective and effective photo-degradation of the water contaminant used as a template.

In view of real applications, it is crucial to examine the eventual toxicity of the investigated materials. For this reason, we have tested the micro/nanopowders toxicity using the zebrafish as model organism (see details in the supporting information Fig. S13). The obtained positive results lead to exclude, with the investigated experimental conditions, a critical toxicity of the examined materials.

4. Conclusions

Molecularly imprinted TiO_2 photocatalysts were synthesized using an easy and simple sol-gel methodology. The herbicide 2,4-D or the insecticide imidacloprid, two common pesticides in agriculture, were used as templates during the synthesis process, and then removed through a calcination step. The effectiveness of the molecular imprinting processes was confirmed by FTIR and XPS measurements, that highlighted the formation of electrostatic interaction and/or hydrogen bonds between the Ti–O–Ti network and the pesticide molecules in the first steps of the sol-gel synthesis. This approach induced an increased and selective photodegradation of the water contaminant used as a template, i.e. TiO_2 MI/2,4D sample towards the degradation of 2,4D, and TiO_2 MI/Imid sample towards the degradation of imidacloprid. Finally, the eventual toxicity of the synthesized TiO_2 powders was excluded thanks to the positive responses of the

zebrafish embriotoxicity tests. The approach described is a promising strategy to obtain safe and performing materials for environmental applications.

Acknowledgments

This work was partially funded by the SENTI project, ESF (European Social Found) Sicily 2020 (CUP: G67B17000160009). We want to thank Andrea Zappavigna (Materials S.r.l. of Rome) for N_2 adsorption-desorption measurements, Riccardo Reitano (University of Catania) for the support in FTIR analyses, and Giuseppe Pantè (CNR-IMM) for the technical assistance. A.G. thanks the University of Catania (Piano della Ricerca di Ateneo 2016-2018) for the financial support.

References

[1] F.P. Carvalho, Pesticides, environment, and food safety, Food Energy Secur. 6 (2017) 48-60.

[2] L.M. Chiesa, G.F. Labella, A. Giorgi, S. Panseri, R. Pavlovic, S. Bonacci, F. Ariol, The occurrence of pesticides and persistent organic pollutants in Italian organic honeys from different productive areas in relation to potential environmental pollution, Chemosphere 154 (2016) 482-490.

[3] K.H. Kim, E. Kabir, S.A. Jahan, Exposure to pesticides and the associated human health effects, Sci. Total Environ. 575 (2017) 525-535.

[4] M. Arias-Estevez, E. Lopez-Periago, E. Martınez-Carballo, J. Simal-Gandara, J.C. Mejuto, L- Garcıa-Rio, The mobility and degradation of pesticides in soils and the pollution of groundwater resources, Agric. Ecosyst. Environ. 123 (2008) 247-260.

[5] V. Ghormade, M.V. Deshpande, K.M. Paknikar, Perspectives for nano-biotechnology enabled protection and nutrition of plants, Biotechnol. Adv. 29 (2011) 792-803.

[6] A. Di Mauro, M. Cantarella, G. Nicotra, V. Privitera, G. Impellizzeri, Low temperature atomic layer deposition of ZnO: applications in photocatalysis, Appl. Catal. B: Environ. 196 (2016) 68-76.

[7] V. Scuderi, G. Impellizzeri, M. Zimbone, R. Sanz, A. Di Mauro, A. Buccheri, M.P. Miritello, A. Terrasi, G. Rappazzo, G. Nicotra, V. Privitera, Rapid synthesis of photoactive hydrogenated TiO_2 nanoplumes, Appl. Catal. B: Environ. 183 (2016) 328-334.

[8] E. Greco, E. Ciliberto, A.M.E. Cirino, D. Capitani, V. Di Tullio, A new preparation of doped photocatalytic TiO_2 anatase nanoparticles: a preliminary study for the removal of pollutants in confined museum areas, Appl. Phys. A 122 (2016) 530.

[9] N. Vela, M. Calína, M.J. Yáñez-Gascón, Isabel Garrido, G. Pérez-Lucas, J. Fenoll, S. Navarro, Photocatalytic oxidation of six pesticides listed as endocrine disruptor chemicals from wastewater using two different TiO_2 samples at pilot plant scale under sunlight irradiation, J. Photochem. Photobiol. A 353 (2018) 271-278.

[10] C. Guillard, J. Disdier, C. Monnet, J. Dussaud, S. Malato, J. Blanco, M.I. Maldonado, J.M. Herrmann, Solar efficiency of a new deposited titania photocatalyst: chlorophenol, pesticide and dye removal applications, Appl. Catal. B: Environ. 46 (2003) 319-332.

[11] V. Scuderi, G. Impellizzeri, L. Romano, M. Scuderi, M.V. Brundo, K. Bergum, M. Zimbone, R. Sanz, M.A. Buccheri, F. Simone, G. Nicotra, B.G. Svensson, M.G. Grimaldi, V. Privitera, An enhanced photocatalytic response of nanometric TiO_2 wrapping of Au nanoparticles for eco-friendly water applications, Nanoscale 6 (2014) 11189-11195.

[12] R. Fiorenza, M. Bellardita, T. Barakat, S. Scirè, L. Palmisano, Visible light photocatalytic activity of macro-mesoporous TiO_2-CeO_2 inverse opals, J. Photochem. Photobiol. A 352 (2018) 25-34.

[13] R. Fiorenza, M. Bellardita, S. Scirè, L. Palmisano, Effect of the addition of different doping agents on visible light activity of porous TiO_2 photocatalysts, Molecular Catalysis 455 (2018) 108-120.

[14] M. Pedrosa, L. M. Pastrana-Martínez, M. F. R. Pereira, J. L. Faria, J. L. Figueiredo, A. M.T. Silva, N/S-doped graphene derivatives and TiO_2 for catalytic ozonation and photocatalysis of water pollutants, Chem. Eng. J. 348 (2018) 888-897.

[15] M. Zimbone, G. Cacciato, M. Boutinguiza, A. Gulino, M. Cantarella, V. Privitera, M. G. Grimaldi, Hydrogenated black-TiO_x: a Facile and Scalable Synthesis for Environmental Water Purification. Catal. Today 321-322 (2019) 146-157.

[16] M. Zimbone, G. Cacciato, R. Sanz, R.Carles, A. Gulino, V. Privitera, M. G. Grimaldi, Black TiO_x photocatalyst obtained by laser irradiation in water, Catal. Commun, 84 (2016) 11–15.

[17] M. Zimbone, G. Cacciato, L. Spitaleri, R. G. Egdell, M. G. Grimaldi, A. Gulino, Sb-Doped Titanium Oxide: A Rationale for Its Photocatalytic Activity for Environmental Remediation, ACS Omega 3 (2018) 11270−11277.

[18] Y. Jiang, H. Ning, C. Tian, B. Jiang, Q. Li, H. Yan, X. Zhang, J. Wang, L. Jing, H. Fu, Single-crystal TiO_2 nanorods assembly for efficient and stable cocatalyst-free photocatalytic hydrogen evolution, Appl. Catal. B: Environ. 229 (2018) 1-7.

[19] R. Fiorenza, M. Bellardita, S. Scirè, L. Palmisano, Photocatalytic H_2 production over inverse opal TiO_2 catalysts, Catal. Today 321-322 (2019) 113-119.

[20] M. Tobajas, C. Belver, J.J. Rodriguez, Degradation of emerging pollutants in water under solar irradiation using novel TiO_2-ZnO/clay nanoarchitectures, Chem. Eng. J. 309 (2017) 596-606.

[21] J. Carbajo, M. Jiménez, S. Miralles, S. Malato, M. Faraldos, A. Bahamond, Study of application of titania catalysts on solar photocatalysis: Influence of type of pollutants and water matrices, Chem. Eng. J. 291 (2016) 64-73.

[22] N. Shaham-Waldmannm, Y. Paz, Modified Photocatalysts in Photocatalysis and Water Purification: From Fundamentals to Recent Reports, Wiley,Germany, 2013.

[23] G. Zhang, W. Choi, S.H. Kim, S. B. Hong, Selective photocatalytic degradation of aquatic pollutants by titania encapsulated into FAU-type zeolites, J. Hazard. Mater., 188 (2011) 198-205.

[24] M.A. Lazar, W.A. Daoud, Achieving selectivity in TiO_2-based photocatalysis, RSC Adv. 3 (2013) 4130-4140.

[25] D. Robert, A. Piscopo, J.-V. Weber, First approach of the selective treatment of water by heterogeneous photocatalysis, Environ. Chem. Lett. 2 (2004) 5-8.

[26] S. Miyayama, K. Nishijima, T. Kamai, T. Chiyoya, T. Tsubota, T. Ohno, Photocatalytic selective oxidation of anionic compounds on TiO_2 photocatalysts modified with quaternary ammonium base groups. Sep. Purif. Technol. 58 (2007) 206-210.

[27] K. Inumaru, M. Murashima, T. Kasahara, Enhanced photocatalytic decomposition of 4-nonylphenol by surface organo grafted TiO_2: A combination of molecular selective adsorption and photocatalysis, Appl. Catal. B Environ: 52 (2004) 275-280.

[28] O.V. Makarova, T. Rajh, M.C. Thurnaure, Surface modification of TiO_2 nanoparticles for photochemical reduction of nitrobenzene. Environ. Sci. Technol. 34 (2000) 4797-4803.

[29] Y. Chen, W. Li, J. Wang, Y. Gan, L. Liu, M. Ju, Microwave-assisted ionic liquid synthesis of Ti^{3+} self-doped TiO_2 hollow nanocrystals with enhanced visible-light photoactivity, Appl. Catal. B Environ. 191 (2016) 94-105.

[30] D.S. Bhachu, R.G. Egdell, G.Sankar, C.J. Carmalt, I.P. Parkin, Electronic properties of antimony-doped anatase TiO_2 thin films prepared by aerosol assisted chemical vapour deposition, J. Mater. Chem. C 5 (2017) 9694−9701.

[31] S. Liu, J. Yu, M. Jaroniec, Tunable photocatalytic selectivity of hollow TiO_2 microspheres composed of anatase polyhedra with exposed {001} facets. J. Am. Chem. Soc. 132 (2010) 11914-11916.

[32] M.V. Polyakov, Adsorption properties and structure of silica gel. Zh. Fiz. Khim. 2 (1931) 799–804.

[33] A. Katz, M.E. Davis, Molecular imprinting of bulk, microporous silica, Nature 403 (2000) 286-289.

[34] X. Shen, L. Zhu, N. Wang, L. Ye, H. Tang, Molecular imprinting for removing highly toxic organic pollutants, Chem. Commun. 48 (2012) 788-798.

[35] C. Huang, Z. Tu, X. Shen, Molecularly imprinted photocatalyst with a structural analogue of template and its application, J. Hazard. Mater. 248– 249 (2013) 379-386.

[36] M. Cantarella, A. Di Mauro, A. Gulino, L. Spitaleri, G. Nicotra, V. Privitera, G. Impellizzeri, Selective photodegradation of paracetamol by molecularly imprinted ZnO nanonuts, Appl. Catal. B Environ. 238 (2018) 509-517.

[37] M. Cantarella, G. Impellizzeri, V. Privitera, Functional nanomaterials for water purification, Riv. Nuovo Cimento 40 (2017) 595-632.

[38] C. Coelho de Escobar, M. Azário Lansarina, J. Henrique Zimnoch dos Santos, Synthesis of molecularly imprinted photocatalysts containing low TiO_2 loading:

Evaluation for the degradation of pharmaceuticals J. Hazard. Mater. 306 (2016) 359-366.

[39] C. Lai, M.M Wang, G.M. Zeng, Y.G. Liu, D.L. Huang, C. Zhang, R.Z. Wang, P. Xu, M. Cheng, C. Huang, H.P. Wu, L. Qin, Synthesis of surface molecular imprinted TiO_2/graphene photocatalyst and its highly efficient photocatalytic degradation of target pollutant under visible light irradiation, Appl. Surf. Sci. 390 (2016) 368-376.

[40] X. Shen, L. Zhu, H. Yu, H. Tang, S. Liu, W. Li, Selective photocatalysis on molecular imprinted TiO_2 thin films prepared via an improved liquid phase deposition method, New J. Chem. 33 (2009) 1673-1679.

[41] Z. Lu, F. Chen, M. He, M. Song, Z. Ma, W. Shi, Y. Yan, J. Lan, F. Li, P. Xiao, Microwave synthesis of a novel magnetic imprinted TiO_2 photocatalyst with excellent transparency for selective photodegradation of enrofloxacin hydrochloride residues solution, Chem. Eng. J. 249 (2014) 15-26.

[42] D. Carboni, L. Malfatti, A. Pinna, B. Lasio, Y. Tokudome, M. Takahashi, P. Innocenzi, Molecularly imprinted La-doped mesoporous titania films with hydrolytic properties toward organophosphate pesticides, New J. Chem. 37 (2013) 2995-3002.

[43] Y.N. Zhang, W. Dai, Y. Wen, G. Zhao, Efficient enantioselective degradation of the inactive (S)-herbicide dichlorprop on chiral molecular-imprinted TiO_2, Appl. Catal. B Environ. 212 (2017) 185-192.

[44] F. Deng, Y. Liu, X. Luo, S. Wu, S. Luo, C. Au, R. Qi, Sol-hydrothermal synthesis of inorganic-framework molecularly imprinted TiO_2/SiO_2 nanocomposite and its preferential photocatalytic degradation towards target contaminant, J. Hazard. Mater. 278 (2014) 108-115.

[45] X. Shen, L. Zhu, C. Huang, H. Tang, Z. Yu, F. Deng, Inorganic molecular imprinted titanium dioxide photocatalyst: synthesis, characterization and its application for efficient and selective degradation of phthalate esters, J. Mater. Chem. 19 (2009) 4843-4851.

[46] D.M. Han, G.L. Dai, W.P. Jia, H.D. Liang, Preparation and photocatalytic activity of Cu^{2+}-doped 2,4-dichlorophenol molecularly imprinted SiO_2-TiO_2 nanocomposite, Micro. Nano. Lett. 5 (2010) 76-80.

[47] S. Xu, H. Lu, L. Chen, X. Wang, Molecularly imprinted TiO_2 hybridized magnetic Fe_3O_4 nanoparticles for selective photocatalytic degradation and removal of estrone, RSC Adv. 4 (2014) 45266-45274.

[48] D. Sharabi, Y. Paz, Preferential photodegradation of contaminants by molecular imprinting on titanium dioxide, Appl. Catal. B: Environ. 95 (2010) 169-178.

[49] X. Luo, F. Deng, L. Min, S. Luo, B. Guo, G. Zeng, C. Au, Facile One-Step Synthesis of Inorganic-Framework Molecularly Imprinted TiO_2/WO_3 Nanocomposite and Its Molecular Recognitive Photocatalytic Degradation of Target Contaminant, Environ. Sci. Technol. 47 (2013) 7404-7412.

[50] Y. Song, C. Rong, J. Shang, Y. Wang, Y. Zhang, K. Yu, Synthesis of an inorganic-framework molecularly imprinted Fe-doped TiO_2 composite and its selective photo-Fenton-like degradation of acid orange II, J. Chem. Technol. Biotechnol. 92 (2017) 2038-2049.

[51] Y. Wu, Y. Dong, X. Xia, X. Liu, H. Li, Facile synthesis of N-F codoped and molecularly imprinted TiO_2 for enhancing photocatalytic degradation of target contaminants, App. Surf. Sci. 364 (2016) 829-836.

[52] S. Ahmed, M.G. Rasul, R. Brown, M.A. Hashib, Influence of parameters on the heterogeneous photocatalytic degradation of pesticides and phenolic contaminants in wastewater: A short review, J. Enviro. Manage. 92 (2011) 311-330.

[53] M.J.Farre´, M.I. Franch, S.Malato, J.A. Ayllon, J. Peral, X. Domenech, Degradation of some biorecalcitrant pesticides by homogeneous and heterogeneous photocatalytic ozonation, Chemosphere 58 (2005) 1127-1133.

[54] Tomlin, The pesticide manual. 10th ed. Boca Raton: Crop Protection Publications; 1994.

[55] G. Shuai Jiang, S.A. Zhong, L. Chen, I. Blakey, A. Whitaker, Synthesis of molecularly imprinted organic-inorganic hybrid azobenzene materials by sol-gel for radiation induced selective recognition of 2,4-dichlorophenoxyacetic acid, Radiat. Phys. Chem. 80 (2011) 130-135.

[56] D. Fonseca MB, L. Glusczak, B.S. Moraes, D. Menezes, A. Pretto, M.A. Tierno, R.Zanella, F.F. Goncalves, V.L. Loro, Ecotoxicol. The 2,4-D herbicide effects on acetylcholinesterase activity and metabolic parameters of piava freshwater fish (Leporinus obtusidens), Environ. Saf. 69 (3) (2008) 416-420.

[57] M. Tomizawa, J.E. Casida, Neonicotinoid Insecticides: Highlights of a Symposium on Strategic Molecular Designs, J. Agric. Food Chem. 59 (2010) 2883-2886.

[58] D. Ozsahin, R. Bal, O. Yılmaz, Biochemical alterations in kidneys of infant and adult male rats due to exposure to the neonicotinoid insecticides imidacloprid and clothianidin, Toxicol. Res. 3 (2014) 324-330.

[59] S.P. Pandey, B. Mohanty, The neonicotinoid pesticide imidacloprid and the dithiocarbamate fungicide mancozeb disrupt the pituitary–thyroid axis of a wildlife bird, Chemosphere, 122 (2015) 227-234.

[60] W. Ge, S. Yan, J. Wang, L. Zhu, A. Chen, J. Wang, Oxidative Stress and DNA Damage Induced by Imidacloprid in Zebrafish (*Danio rerio*), J. Agric. Food Chem. 63 (2015) 1856-1862

[61] OECD, 2013. Guideline for the Testing of Chemicals Fish Embryo Toxicity (FET). Test. Paris: OECD. Available online at: <www.oecd.org>.

[62] M.R. Embry, S.E. Belanger, T.A. Braunbeck, M. Galay-Burgos, M. Halder, D.E. Hinton, M.A. Léonard, A. Lillicrap, T. Norberg-King, G. Whale The fish embryo toxicity test as an animal alternative method in hazard and risk assessment and scientific research. Aquat. Toxicol. 97 (2010) 79-87.

[63] M.V. Brundo, R. Pecoraro, F. Marino, A. Salvaggio, D. Tibullo, S. Saccone, V. Bramanti, M.A. Buccheri, G. Impellizzeri, V. Scuderi, M. Zimbone, V. Privitera. Toxicity evaluation of new engineered nanomaterials in zebrafish Front. Physiol. 7 (2016) 130.

[64] R. Pecoraro, A. Salvaggio, F. Marino, G. Di Caro, F. Capparucci, B.M. Lombardo, G. Messina, E.M. Scalisi, M. Tummino, F. Loreto, G. D'Amante, R. Avola, D. Tibullo, M.V. Brundo. Metallic nano-composite toxicity evaluation by zebrafish embryo toxicity test with identification of specific exposure biomarkers. Curr. Protoc. Toxicol. 74 (2017), 1.14.1–14.1.13.

[65] R. Pecoraro., D. D'Angelo, S. Filice, S. Scalese, F. Capparucci, F. Marino, C. Iaria, G. Guerriero., D. Tibullo, E.M. Scalisi., A. Salvaggio, I. Nicotera, M.V. Brundo. Toxicity Evaluation of Graphene Oxide and Titania Loaded Nafion Membranes in Zebrafish. Front Physiol. 2018 4:8:1039; doi: 10.3389/fphys.2017.01039.

[66] R. Pecoraro, F. Marino, A. Salvaggio, F. Capparucci, G. Di Caro, C. Iaria, A. Salvo, A. Rotondo, D. Tibullo, G. Guerriero, E.M. Scalisi, M. Zimbone, G,

Impellizzeri, M.V. Brundo. Evaluation of chronic nanosilver toxicity to adult zebrafish. Front. Physiol. 2017 14:8:1011. doi: 10.3389/fphys.2017.01011C.

[67] M.E. Diaz-Garcıa, R.B. Laino, Molecular Imprinting in Sol-Gel Materials: Recent Developments and Applications, Microchim. Acta 149 (2005) 19-36.

[68] A. Gulino, Structural and Electronic Characterization of Self-assembled Molecular Nanoarchitectures by X-ray Photoelectron Spectroscopy. Anal. Bioanal. Chem. 405 (2013) 1479-1495.

[69] D. Briggs, J. T. Grant, Surface Analysis by Auger and X-Ray Photoelectron Spectroscopy, 2003 IMP, Chichester, UK.

[70] J.S. Noh, J.A. Schwarz, Estimation of the Point of Zero Charge of Simple Oxides by Mass Titration, J. Colloid Interface Sci. 130 (1989) 157-163.

[71] R. Wang, K. Hashimoto, A. Fujishima, M. Chikuni, E. Kojima, A. Kitamura, M. Shimohigoshi, T. Watanabe, Light-induced amphiphilic surfaces, Nature 388 (1997) 431–432

[72] A.D. McNaught, A. Wilkinson, Compendium of Chemical Terminology, 2nd edn., Blackwell Scientific Publications, Oxford, 1997 “the Gold Book”.

[73] A. Salvaggio, F. Marino, M. Albano, R. Pecoraro, G. Camiolo, D. Tibullo, V. Bramanti., B.M. Lombardo, S. Saccone, V. Mazzei, M.V.Brundo, Toxic Effects of Zinc Chloride on the Bone Development in Danio rerio (Hamilton, 1822). Front Physiol. (2016) 29;7:153. doi: 10.3389/fphys.2016.00153.

[74] Y. Chen, E. Stathatos, D.D. Dionysiou, Sol-gel modified TiO_2 powder films for high performance dye-sensitized solar cells, J. J. Photochem. Photobiol. A 203 (2009) 192-198.

[75] A.K.L. Sajjad, S. Shamaila, B. Tian, F. Chen, J. Zhang, One step activation of WO_x/TiO_2 nanocomposites with enhanced photocatalytic activity, Appl. Catal. B

Environ. 91 (2009) 397-405.

[76] W. Subramonian, T.Y. Wu, S.P. Chai, Photocatalytic degradation of industrial pulp and paper mill effluent using synthesized magnetic Fe_2O_3-TiO_2: Treatment efficiency and characterizations of reused photocatalyst, J. Environ. Manage. 187 (2017) 298-310.

[77] S.P. Albu, A. Ghicov, S. Aldabergenova, P. Drechsel, D. LeClere, G.E. Thompson, J.M. Macak, P. Schmuki, Formation of Double-Walled TiO_2 Nanotubes and Robust Anatase Membranes, Adv. Mater. 20 (2008) 4135-4139.

[78] K.S. Yoo, T.G. Lee, J. Kim, Preparation and characterization of mesoporous TiO_2 particles by modified sol-gel method using ionic liquids, Microp. Mesop. Mat. 84 (2005) 211-217.

[79] E.P. Barrett, L.G. Joyner, P.P. Halenda, Study of pore size distribution by capillary absorption method, J. Am. Chem. Soc.73 (1951),373-380.

[80] N.S. Trivedi, R.A. Kharkar, S.A. Mandavgane, Utilization of cotton plant ash and char for removal of 2, 4-dichlorophenoxyacetic acid, Resour. Effic. Technol. 2 (2016) S39-S46.

[81] D.L. Pavia, G.M. Lampman, G.S. Kriz, J.R. Vyvyan, Introduction to Spectroscopy, fourth ed., Brooks Cole Cengage Learning, USA, 2008, 46-48.

[82] A. Davydov, Molecular Spectroscopy of Oxide Catalyst Surfaces, in: N.T. Sheppard (Ed.), John Wiley & Sons Ltd, The Atrium, Southern Gate, Chichester, West Sussex PO19 8SQ, England, 2003.

[83] M. Zhang, L. Shi, S. Yuan, Y. Zhao, J. Fang, Synthesis and photocatalytic properties of highly stable and neutral TiO_2/SiO_2 hydrosol J. Coll Int. Sc. 330 (2009), 113-118.

[84] Z. Gao, L. Pang, H. Feng, S. Wang, Q. Wang, M. Wang, Y. Xi, S. Hu, Preparation

and characterization of a novel imidacloprid microcapsule via coating of polydopamine and polyurea, RSC Adv. 7 (2017) 15762-15768.

[85] G. Socrates, Infrared and Raman Characteristic Group Frequencies: Tables and Charts, 3rd ed.; Wiley, New York, 2004.

[86] A. Gulino, A.E. Taverner, S. Warren, P. Harris, R.G. Egdell, A Photoemission Study of Sb-Doped TiO_2. Surf. Sci. 315 (1994) 351-361.

[87] A. Gulino, G.G. Condorelli, I. Fragalà, R.G. Egdell, Surface segregation of Sb in doped TiO_2 rutile. Appl. Surf. Sci. 90 (1995) 289-295.

[88] G. Sivalingam, K. Nagaveni, M.S. Hegde, G. Madras, Photocatalytic degradation of various dyes by combustion synthesized nano anatase TiO_2, Appl. Catal. B: Environ. 45 (2003) 23-38.

[89] S. Eriksen, R.G. Egdell, Electronic Excitations at Oxygen Deficient TiO_2(110) Surfaces: a Study by EELS. Surf. Sci. 180 (1987) 263-278.

[90] R. Sadeghi, V.E. Henrich, Electronic interactions in the rhodium/TiO_2 system J. Catal., 109, (1988) 1-11.

[91] B. Bharti, S. Kumar, H.N. Lee, R. Kumar, Formation of Oxygen Vacancies and Ti^{3+} State in TiO_2 Thin Film and Enhanced Optical Properties by Air Plasma Treatment. Sci. Rep. 6 (2016) 32355.

[92] A. Di Paola, G. Marcı`, L. Palmisano, M. Schiavello, K. Uosaki, S. Ikeda, B. Ohtani, Preparation of Polycrystalline TiO_2 Photocatalysts Impregnated with Various Transition Metal Ions: Characterization and Photocatalytic Activity for the Degradation of 4-Nitrophenol, J. Phys. Chem. B 106 (2002) 637-645.

[93] L. Zang, P. Qu, J. Zhao, T. Shen, H. Hidaka, Photocatalytic bleaching of p-nitrosodimethylaniline in TiO, aqueous suspensions: A kinetic treatment involving some primary events photoiniducedon the particle surface, J. Mol. Catal. A: Chem.

120 (1997) 235-245.

[94] Y.Q. Wu, G.X. Lu, S.B. Li, The Doping Effect of Bi on TiO_2 for Photocatalytic Hydrogen Generation and Photodecolorization of Rhodamine B, J. Phys. Chem. C 113 (2009) 9950–9955.

[95] S. Sandeep, K.L. Nagashree, T. Maiyalagan, G. Keerthiga, Photocatalytic degradation of 2,4-dichlorophenoxyacetic acid - A comparative study in hydrothermal TiO_2 and commercial TiO_2, Appl. Surf. Sci 449 (2018) 371-379.

[96] A.Verma, A.P. Toor, N.T. Prakash, P. Bansal, V.K. Sangal, Stability and durability studies of TiO_2 coated immobilized system for the degradation of imidacloprid, New J. Chem. 41(2017) 6296-6304.

[97] D. Han, W. Jia, H. Liang, Selective removal of 2,4-dichlorophenoxyacetic acid from water by molecularly-imprinted amino-functionalized silica gel sorbent, J. Environ. Sci. 22(2) 237-241.

[98] X. Yang, J. Chen, H. Liu, X. Li, S. Zhong, Molecularly imprinted polymers based on zeolite imidazolate framework-8 for selective removal of 2,4-dichlorophenoxyacetic acid, Colloid Surface A 570 (2019) 244-250.

[99] Y.-Hum Yun, H.-Kyong Shon, S.-Do Yoon, Preparation and characterization of molecularly imprinted polymers for the selective separation of 2,4-dichlorophenoxyacetic acid, J. Mater. Sci. 44 (2009) 6206-6211.

[100] Y. Liu, Y. He, Y. Jin, Y. Huang, G. Liu, R. Zhao, Preparation of monodispersed macroporous core–shell molecularly imprinted particles and their application in the determination of 2,4-dichlorophenoxyacetic acid, J. Chromatogr. A, 1323 (2014) 11-17.

[101] G. Guan, S. Wang, H. Zhou, K. Zhang, R. Liu, Q. Mei, S. Wang, Z. Zhang, Molecularly imprinted polypyrrole nanonecklaces for detection of herbicide

through molecular recognition-amplifying current response, Anal. Chim. Acta 702 (2011) 239-246.

[102] D. Huang, T. Yang, Z. Mo, Q. Guo, S. Quan, C. Luo, L. Liu, Preparation of graphene/TiO_2 composite nanomaterials and its photocatalytic performance for the degradation of 2,4-dichlorophenoxyacetic acid, J. Nanomater. (2016) 11, http://dx.doi.org/10.1155/2016/5858906, Article ID 5858906.

[103] H. Chen, Z. Zhang, Z. Yang, Q. Yang, B. Li, Z. Bai, Heterogeneous fenton-like catalytic degradation of 2,4-dichlorophenoxyacetic acid in water with FeS, Chem. Eng. J. 273 (2015) 481-489.

[104] V. Kitsiou, N. Filippidis, D. Mantzavinos, I. Poulios, Heterogeneous and homogeneous photocatalytic degradation of the insecticide imidacloprid in aqueous solutions, Appl. Catal. B Environ. 86 (2009) 27-35.

[105] E. Selli, C.L. Bianchi, C. Pirola, G. Cappelletti, V. Ragaini, Efficiency of 1,4-dichlorobenzene degradation in water under photolysis, photocatalysis on TiO_2 and sonolysis J. Hazard. Mater. 153 (2008) 1136-1141.

Table 1 BET Surface area (S_{BET}), mean pore diameter (d_p) and pore volume (V_p) of the investigated samples.

Catalysts	**S_{BET} ($m^2 g^{-1}$)**	**d_p(nm)**	**V_p ($cm^3 g^{-1}$)**
TiO_2	59 ± 1	5.1 ± 0.2	0.05 ± 0.02
TiO_2 MI/2,4D	55 ± 1	6.4 ± 0.2	0.14 ± 0.02
TiO_2 MI/Imid.	53 ± 1	9.7 ± 0.2	0.19 ± 0.02

Table 2 Vibrational frequencies of 2,4D and TiO_2 MI/2,4D Not Removed samples.

	2,4D	**TiO_2 MI/2,4D Not Removed**
ν C=O	1736 cm^{-1}	1719 cm^{-1}
ν C=$C_{aromatic}$	1478 cm^{-1}	1476 cm^{-1}
ν C−$H_{alkanes}$	1431 cm^{-1}	1424 cm^{-1}
ν C−O−C_{as}	1312 cm^{-1}	1290 cm^{-1}
ν O−H/C−O	1230 cm^{-1}	1230 cm^{-1}
ν C−O−C_s	1092 cm^{-1}	1081 cm^{-1}
ν C−Cl	642 cm^{-1}	642 cm^{-1}

Table 3 Vibrational frequencies of Imidacloprid and TiO_2 MI/Imid Not Removed samples.

	Imidacloprid	**TiO_2 MI/Imid Not Removed**
ν pyridine	1569 cm^{-1}	1539 cm^{-1}
ν C=N/C−$H_{pyrdine}$	1445 cm^{-1}	1443 cm^{-1}
ν N−$C_{secondary\ amine}$	1288 cm^{-1}	1286 cm^{-1}
ν NO_2 S	1230 cm^{-1}	1230 cm^{-1}
ν C−$Cl_{pyrdine}$	1051 cm^{-1}	1051 cm^{-1}

Table 4 XPS Binding Energies (eV) for the investigated TiO_2 samples.

Sample	C 1s	O 1s	Ti $2p_{3/2,1/2}$	Cl $2p_{3/2,1/2}$	N 1s
TiO_2	258.0	531.1	459.9 465.6	-	-
TiO_2 MI/2,4D Not Removed	285.0 289.2	531.7	459.3 465.2	200.3 201.9	-
TiO_2 MI/2,4D	285.0 289.1	530.8	459.4 465.2	-	-
TiO_2 MI/Imid. Not Removed	285.0 288.9	531.4	459.1 464.9	200.2 201.8	399.6 405.3
TiO_2 MI/Imid.	285.0 289.1	530.6	459.1 464.9	-	-

Table 5 Kinetic constants of the photocatalytic degradations of 2,4D.

Sample	k (min^{-1}) $\cdot 10^{-4}$
2,4D	1.01 ± 0.06
TiO_2	6.09 ± 0.06
TiO_2 MI/2,4D	36.15 ± 0.06
TiO_2 MI/Imid	6.08 ± 0.06

Table 6 Kinetic constants of the photocatalytic degradations of imidacloprid.

Sample	k (min^{-1}) $\cdot 10^{-4}$
Imidacloprid	1.00 ± 0.06
TiO_2	11.05 ± 0.06
TiO_2 MI/2,4D	11.09 ± 0.06
TiO_2 MI/Imid	22.45 ± 0.06

Table 7 Kinetic constants of the photocatalytic degradations of 2,4D and imidacloprid in the mixed solution (2,4D + imidacloprid).

Sample	**k 2,4D (min^{-1}) $\cdot 10^{-4}$**	**k imid. (min^{-1}) 10^{-4}**
2,4D + imid.	1.01 ± 0.06	0.99± 0.06
TiO_2	7.03 ± 0.06	11.07 ± 0.06
TiO_2 MI/2,4D	39.05 ± 0.06	12.03± 0.06
TiO_2 MI/Imid	8.06 ± 0.06	20.09 ± 0.06

Table 8 Kinetic constants of the photocatalytic degradations of o-phenylphenol pesticide.

Sample	**k o-phenylphenol (min^{-1}) $\cdot 10^{-4}$**
O-phenylphenol	0.98 ± 0.06
TiO_2	7.85 ± 0.06
TiO_2 MI/2,4D	8.71 ± 0.06
TiO_2 MI/Imid	9.81 ± 0.06

Captions to figures

Fig. 1 Molecular structures of 2,4D and imidacloprid.

Fig. 2 SEM images of TiO_2-based materials: (A) TiO_2 together with a high magnification image reported as inset, (B) TiO_2 MI/2,4D, (C) TiO_2 MI/Imid.

Fig. 3 TEM imagines of TiO_2 (A) and TiO_2 MI/2,4D (B). The diffraction patterns of the samples are reported in the insets.

Fig. 4 XRD patterns of TiO_2, TiO_2 MI/2,4D, and TiO_2 MI/Imid samples (from the bottom to the top).

Fig. 5 Pore size distribution of TiO_2, TiO_2 MI/2,4D, and TiO_2 MI/Imid samples (from the bottom to the top).

Fig. 6 FTIR spectra of (A) 2,4D, TiO_2 MI/2,4D Not Removed, TiO_2 MI/2,4D and TiO_2 (from the bottom to the top) and of (B) imidacloprid TiO_2 MI/Imid. Not Removed, TiO_2 MI/Imid and TiO_2. The dashed lines are the main bands of 2,4D and imidacloprid molecules.

Fig. 7 (A) Al Kα excited XPS of the TiO_2 MI/2,4D sample measured in the Ti 2p binding energy region, (B) Al Kα excited XPS of the TiO_2 MI/2,4D sample measured in the O 1s binding energy region, (C) Al Kα excited XPS of the TiO_2 MI/Imid sample measured in the Ti 2p binding energy region, (D) Al Kα excited XPS of TiO_2 MI/Imid sample, measured in the O 1s binding energy region. In all the spectra the structure due to satellite radiation has been subtracted.

Fig. 8 (A) Photocatalytic degradation of 2,4D under UV light irradiation for 2,4 D (down triangles), TiO_2 (triangles), TiO_2 MI/Imid. (circles) and TiO_2 MI/2,4D

(squares). (B) Photocatalytic degradation of imidacloprid under UV light irradiation for imidacloprid (down triangles), TiO_2 (triangles), TiO_2 MI/Imid (circles) and TiO_2 MI/2,4D (squares). The experimental errors are included in the symbols. (C) Comparison between the measured TOC and UV degradation of 2,4D after 3 h of irradiation for TiO_2, TiO_2 MI/ Imid, and TiO_2 MI/2,4D samples. (D) Comparison between the measured TOC and UV degradation of imidacloprid after 3 h of irradiation for TiO_2, TiO_2 MI/ Imid, and TiO_2 MI/2,4D sample.

Fig. 9 (A) 2,4D photodegradation kinetic constants for TiO_2, TiO_2 MI/Imid and TiO_2 MI/2,4D samples for 5 runs; (B) Imidacloprid photodegradation kinetic constants for TiO_2, TiO_2 MI/Imid and TiO_2 MI/2,4D samples for 5 runs.

Fig. 10 (A) Photocatalytic degradation of 2,4D in the mixed 2,4D + imidacloprid solution under UV light irradiation, for 2,4 D (down triangles), TiO_2 (triangles), TiO_2 MI/Imid. (circles) and TiO_2 MI/2,4D (squares). (B) Photocatalytic degradation of imidacloprid in the mixed 2,4D + imidacloprid solution under UV light irradiation, for imidacloprid (down triangles), TiO_2 (triangle), TiO_2 MI/Imid (circle), and TiO_2 MI/2,4D (square). The experimental errors are within the symbols.

Fig. 11 (A) Molecular structure of ortho-phenylphenol, (B) Photocatalytic degradation of ortho-phenylphenol under UV light irradiation for o-phenylphenol (down triangles), TiO_2 (triangles), TiO_2 MI/Imid. (circles), and TiO_2 MI/2,4D (squares). The experimental errors are within the symbols.

Fig. 12 (A) Molecular structure of 1,4-dichlorobenzene, (B) Photocatalytic degradation of 1,4-dichlorobenzene under UV light irradiation for 1,4-dichlorobenzene (down triangles), TiO_2 (triangles), TiO_2 MI/Imid. (circles),

and TiO_2 MI/2,4D (squares). The experimental errors are within the symbols.

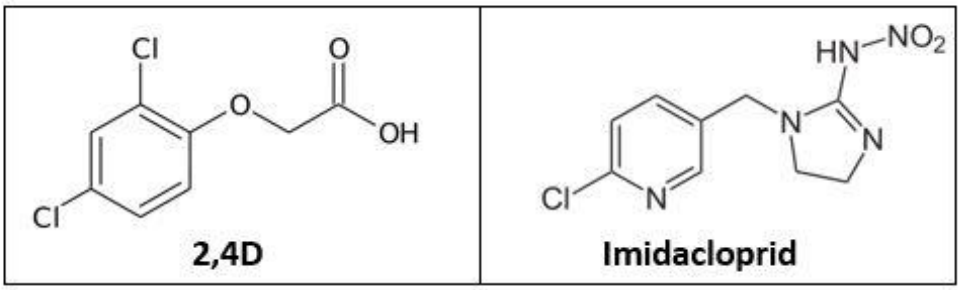

Fig.1

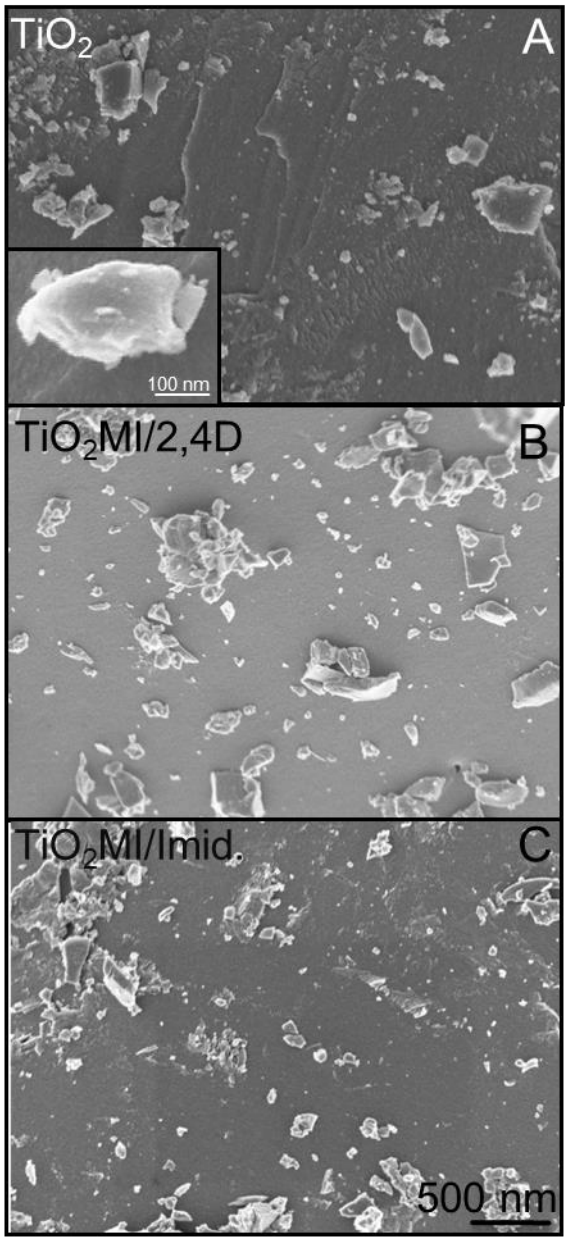

Fig. 2

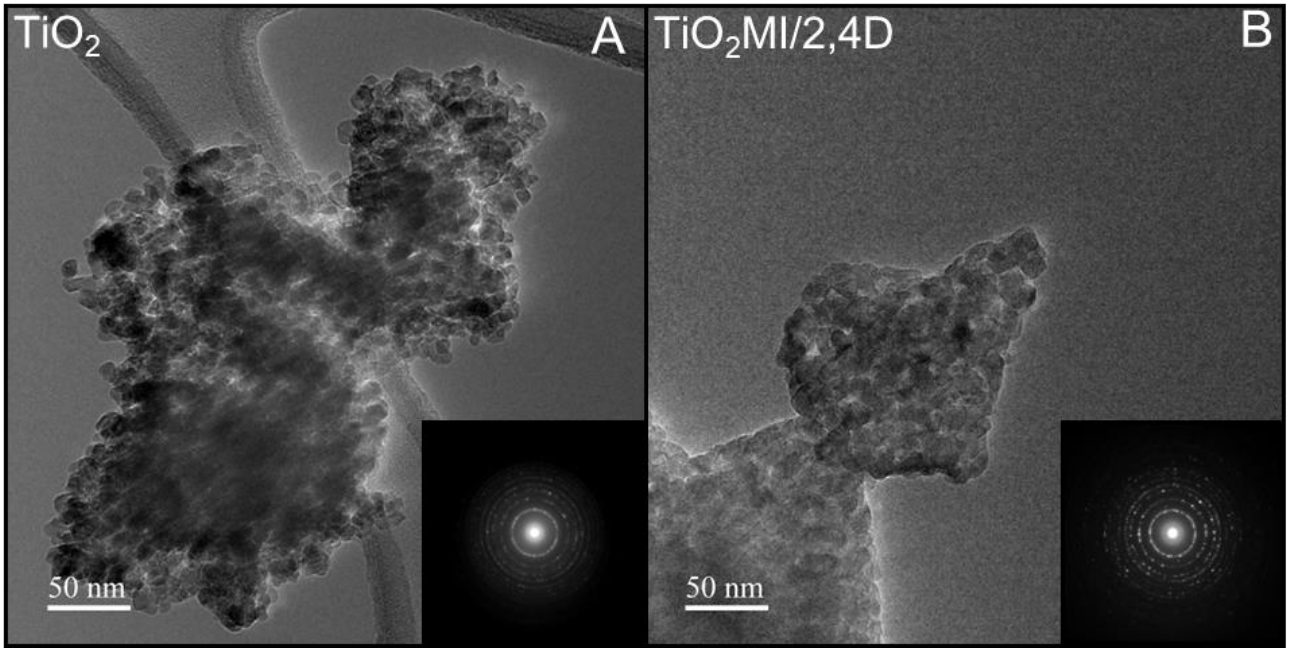

Fig. 3

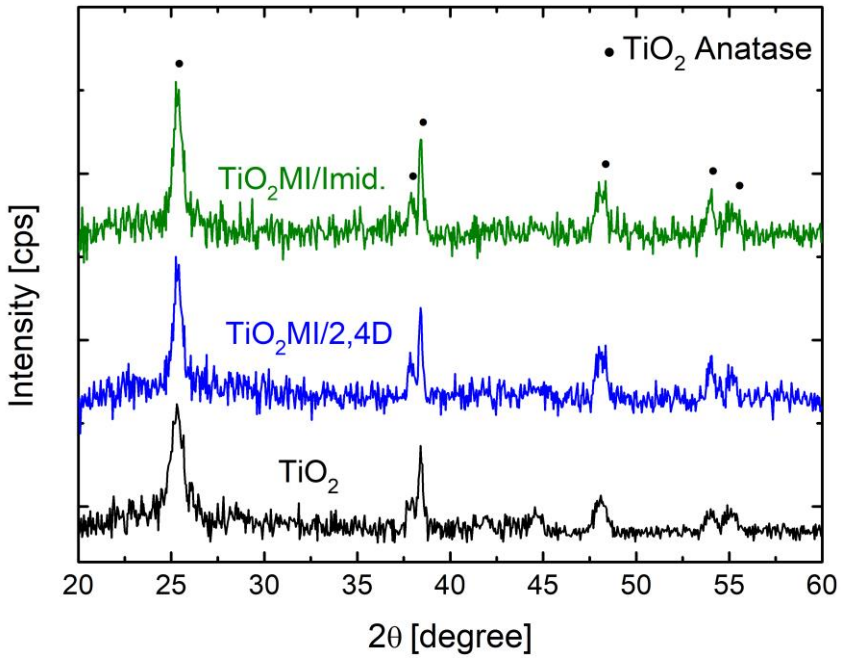
• TiO2 Anatase
TiO2MI/Imid.
TiO2MI/2,4D
TiO2
Intensity [cps]
20
25
30
35
40
45
50
55
60
2θ [degree]

Fig. 4

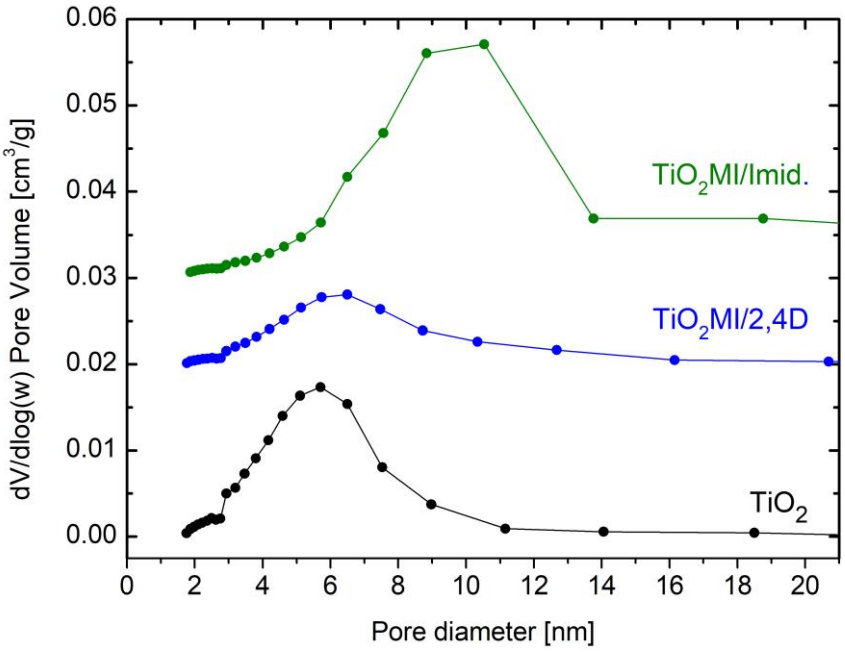
0.06
0.05
0.04
0.03
0.02
0.01
0.00
dV/dlog(w) Pore Volume [cm3/g]
TiO2MI/Imid.
TiO2MI/2,4D
TiO2
0
2
4
6
8
10
12
14
16
18
20
Pore diameter [nm]

Fig. 5

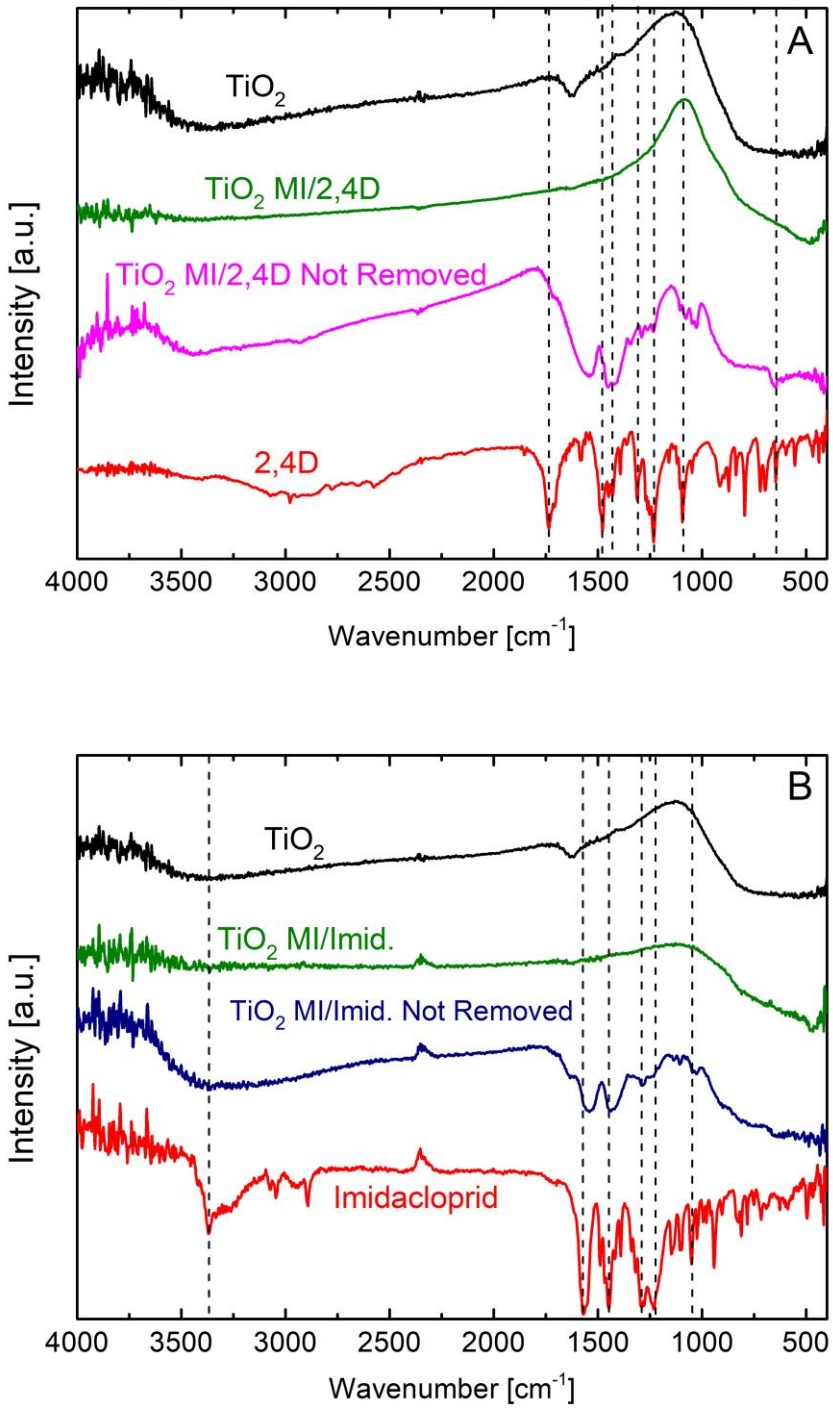
A
TiO2
TiO2 MI/2,4D
TiO2 MI/2,4D Not Removed
2,4D
Intensity [a.u.]
4000 3500 3000 2500 2000 1500 1000 500
Wavenumber [cm-1]
B
TiO2
TiO2 MI/Imid.
TiO2 MI/Imid. Not Removed
Imidacloprid
Intensity [a.u.]
4000 3500 3000 2500 2000 1500 1000 500
Wavenumber [cm-1]

Fig. 6

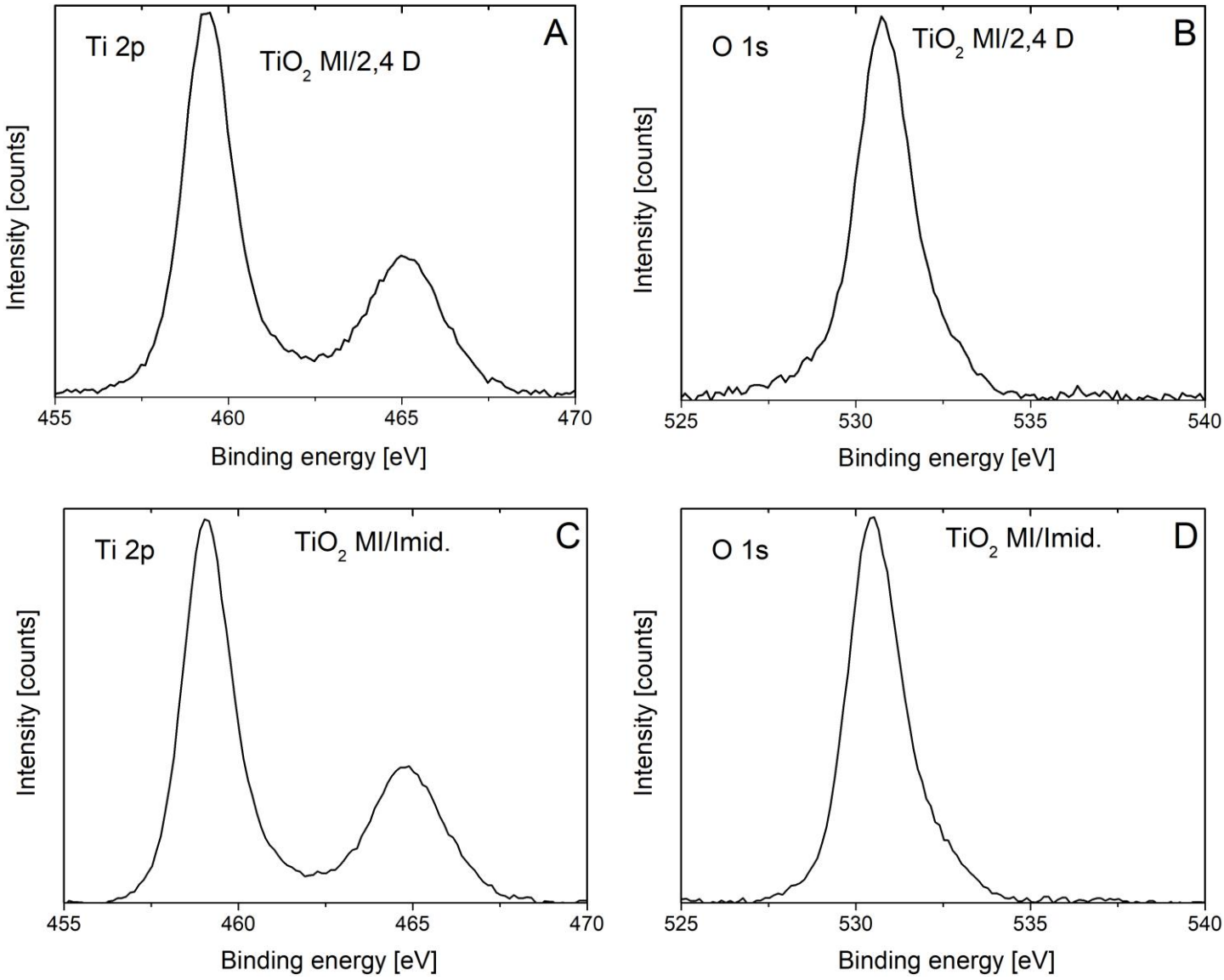
Ti 2p
TiO2 MI/2,4 D
A
Intensity [counts]
455
460
465
470
Binding energy [eV]
O 1s
TiO2 MI/2,4 D
B
Intensity [counts]
525
530
535
540
Binding energy [eV]
Ti 2p
TiO2 MI/Imid.
C
Intensity [counts]
455
460
465
470
Binding energy [eV]
O 1s
TiO2 MI/Imid.
D
Intensity [counts]
525
530
535
540
Binding energy [eV]

Fig. 7

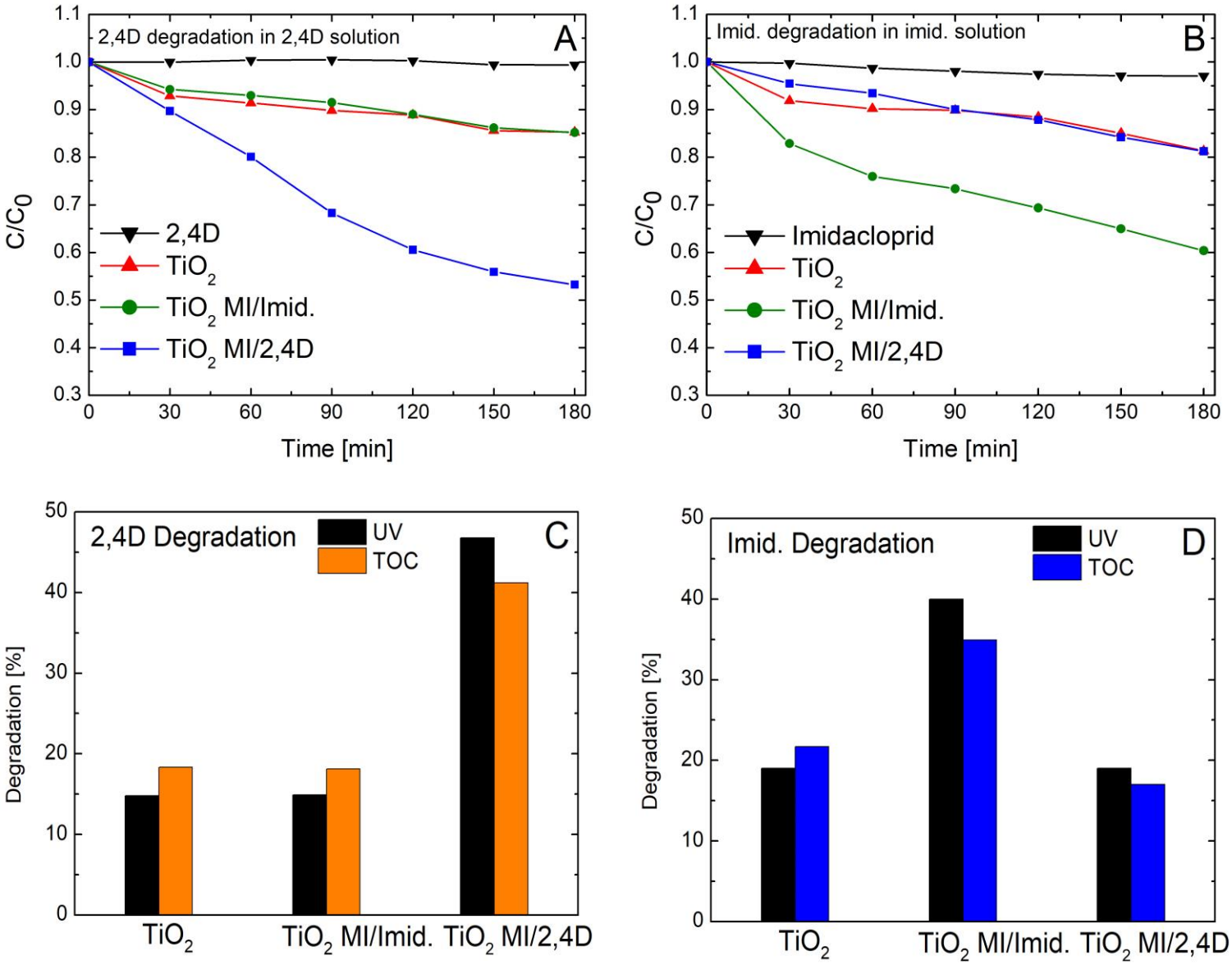
2,4D degradation in 2,4D solution
A
C/C0
Time [min]
2,4D
TiO2
TiO2 MI/Imid.
TiO2 MI/2,4D
Imid. degradation in imid. solution
B
Imidacloprid
2,4D Degradation
C
UV
TOC
Degradation [%]
TiO2
TiO2 MI/Imid.
TiO2 MI/2,4D
Imid. Degradation
D

Fig. 8

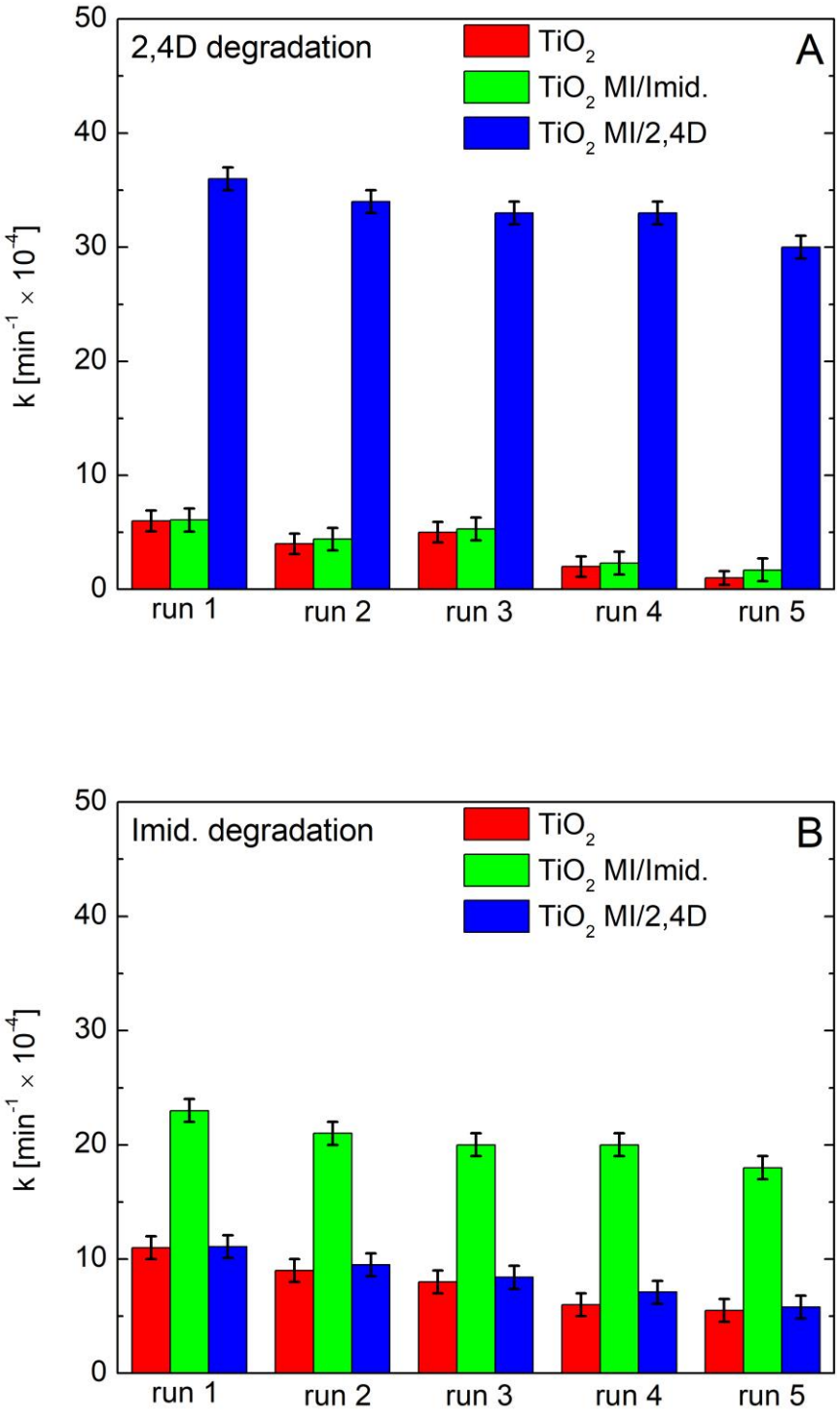
2,4D degradation
A
TiO2
TiO2 MI/Imid.
TiO2 MI/2,4D
k [min-1 × 10-4]
0
10
20
30
40
50
run 1
run 2
run 3
run 4
run 5
Imid. degradation
B
TiO2
TiO2 MI/Imid.
TiO2 MI/2,4D
k [min-1 × 10-4]
0
10
20
30
40
50
run 1
run 2
run 3
run 4
run 5

Fig. 9

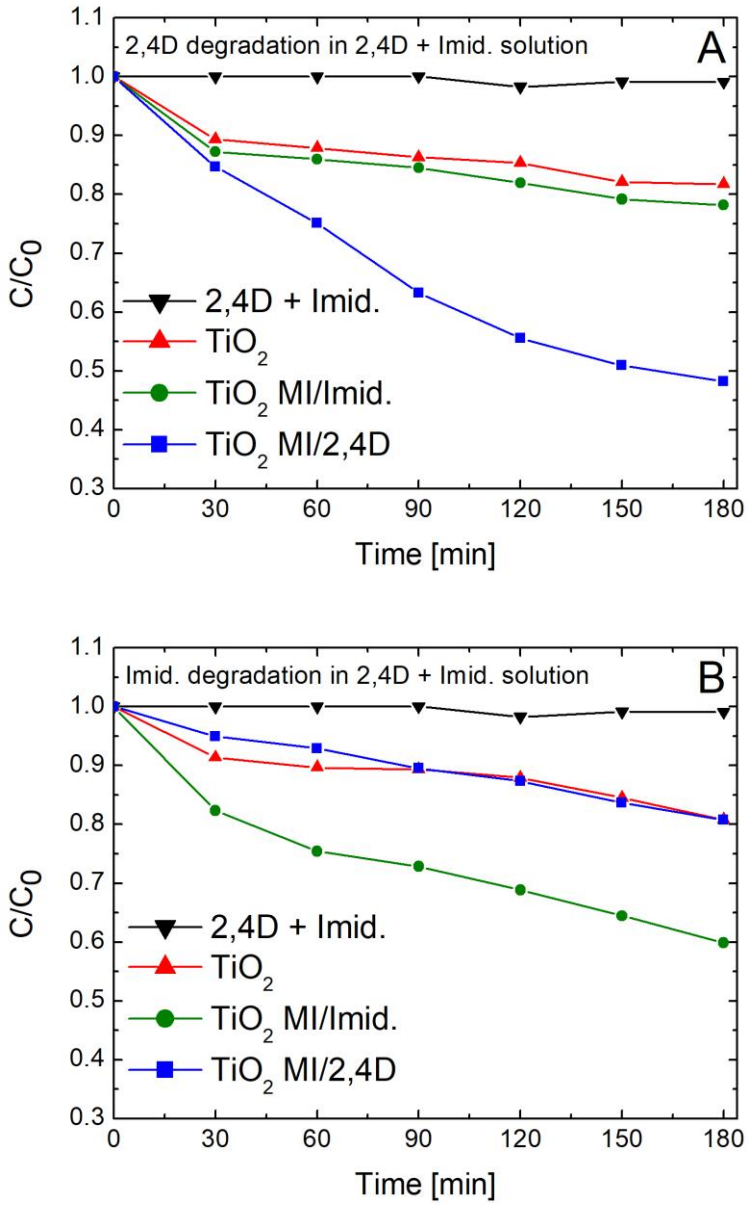
2,4D degradation in 2,4D + Imid. solution
A
C/C0
Time [min]
2,4D + Imid.
TiO2
TiO2 MI/Imid.
TiO2 MI/2,4D
Imid. degradation in 2,4D + Imid. solution
B
C/C0
Time [min]
2,4D + Imid.
TiO2
TiO2 MI/Imid.
TiO2 MI/2,4D

Fig. 10

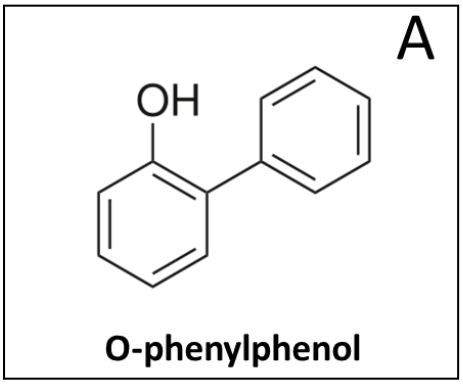
A
OH
O-phenylphenol

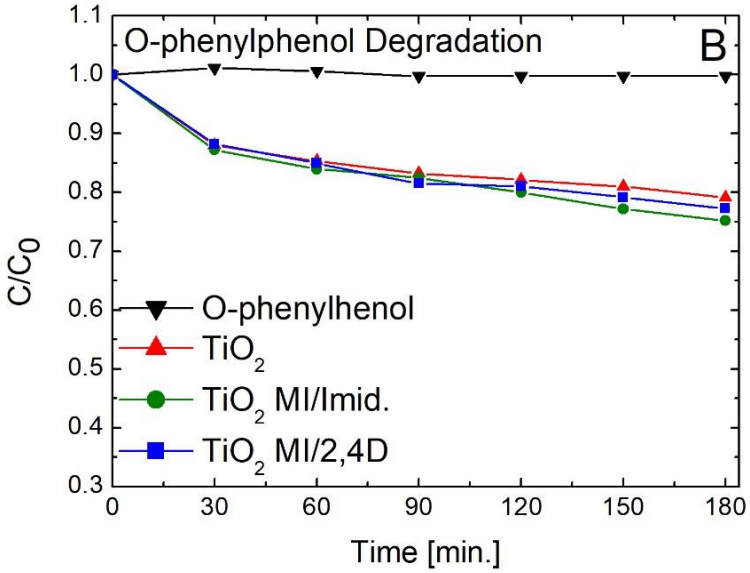
O-phenylphenol Degradation
B
C/C0
Time [min.]
O-phenylhenol
TiO2
TiO2 MI/Imid.
TiO2 MI/2,4D
1.1
1.0
0.9
0.8
0.7
0.6
0.5
0.4
0.3
0
30
60
90
120
150
180

Fig. 11

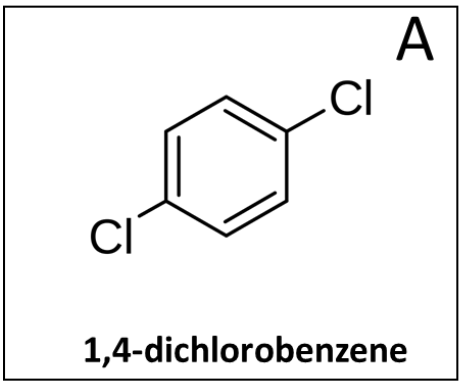
A
Cl
Cl
1,4-dichlorobenzene

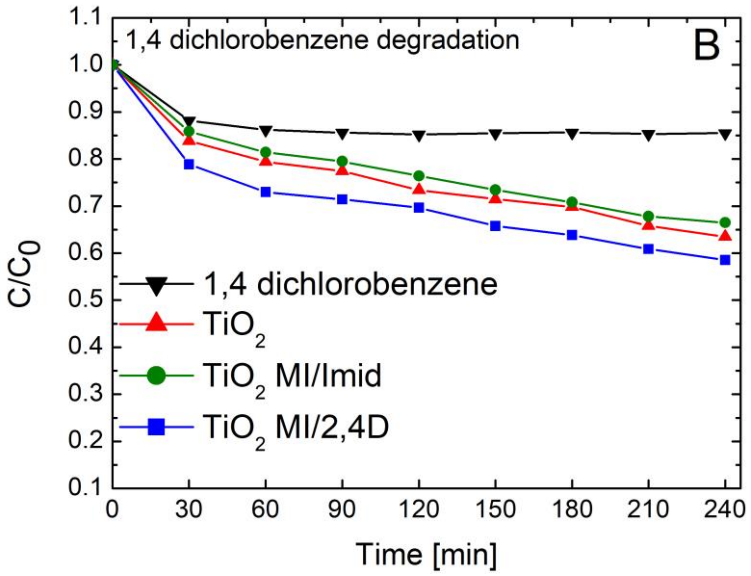
1,4 dichlorobenzene degradation
B
C/C0
1.1
1.0
0.9
0.8
0.7
0.6
0.5
0.4
0.3
0.2
0.1
0
30
60
90
120
150
180
210
240
Time [min]
1,4 dichlorobenzene
TiO2
TiO2 MI/Imid
TiO2 MI/2,4D

Fig. 12